Climatology of the Simulated Great Plains Low-Level Jet and Its Contribution to the Continental Moisture Budget of the United States

H. MARK HELFAND AND SIEGFRIED D. SCHUBERT

Data Assimilation Office, Laboratory for Atmospheres, NASA/Goddard Space Flight Center, Greenbelt, Maryland

(Manuscript received 25 February 1994, in final form 8 August 1994)

ABSTRACT

The Great Plains region of the United States is characterized by some of the most frequent and regular occurrences of a nocturnal low-level jet (LLJ). While the LLJ is generally confined to the lowest kilometer of the atmosphere, it may cover a substantial region of the Great Plains, and typically reaches maximum amplitudes of more than 20 m s^{-1}.

A two-month, springtime simulation with the Goddard Earth Observing System (GEOS-1) atmospheric general circulation model (AGCM) has produced a Great Plains LLJ with a vertical and temporal structure, directionality, and climatological distribution that compare favorably with observations. The diurnal cycle of the low-level flow is dramatic and coherent over a subcontinental area that includes much of the western United States and northern Mexico. This cycle can be interpreted as the nightly intrusion of the anticyclonic, subtropical gyre (associated with the Bermuda high) into the North American continent as surface friction decreases. The AGCM also simulates a pair of northerly LLJ maxima off the California coast, which seem to correspond to observations of a so-called "Baja Jet." Other apparently related diurnal variations extending well into the upper troposphere are documented and compared with observations.

The time-averaged climatological picture of the low-level flow is dominated over land by the nocturnal phase of the diurnal cycle, in which surface friction is minimal and wind speeds are strongest. This pattern, with its zones of strong convergence, is characteristic of an unsteady, strongly forced flow. Over the open ocean, the mean low-level flow is more reminiscent of a smooth, climatological pattern.

Analysis of the simulated moisture budget for the continental United States reveals a horizontally confined region of strong southerly moisture transport with a strong diurnal cycle in the region of the Great Plains LLJ, as has been found in observations of water vapor transport. The LLJ plays a key role in that budget by transporting almost one-third of all the moisture that enters the continental United States with most of the influx from the LLJ (slightly less than two-thirds of it) entering during the 12 nighttime hours. However, it is the mean flow pattern and not covariances associated with the diurnal cycle that contribute most significantly to the total time-mean moisture transport. Covariances on the synoptic and longer timescales contribute only about one-fifth of the total time-mean transport of moisture in the jet region, and covariances on the diurnal timescale are negative and negligible despite the strong diurnal signal in the wind.

1. Introduction

The Great Plains region of the United States is characterized by the frequent formation of a nocturnal low-level jet (LLJ). This jet, which has often been associated with severe weather events, is one of several topographically bound, low-level jets found throughout the globe. The Great Plains LLJ has been documented in a number of observational studies. Means (1954), for example, charted a cross section between Albuquerque, New Mexico, and Little Rock, Arkansas, of a southerly LLJ that occurred during the period 10–12 July 1951. Izumi and Barad (1963) discussed the evolution of a LLJ recorded at Cedar Hill, Texas, on the night of 22/23 February 1961. Hoecker (1963, 1965) analyzed observations from 13 pilot balloon stations between Amarillo, Texas, and Little Rock, Arkansas. The results from three cases during April and May of 1961 showed that the jet maxima occurred between 300 and 800 m, with nighttime wind speeds that could be nearly double that of the sea level geostrophic wind. Bonner (1968) presented a climatology of the LLJ over the United States using two years of rawinsonde station reports. He found that jets occurred most frequently over the Great Plains. The jets in the southern to central Great Plains were generally oriented from the southerly to the southwesterly direction and occurred most often during the six months from April to September. While jets were found at all times of the day, there was a pronounced diurnal signal with the strongest and best defined jets occurring predominantly during the nighttime. The LLJ had a large horizontal scale extending, at times, northward across much of the Great Plains

Corresponding author address: Dr. H. Mark Helfand, Laboratory for the Atmospheres, NASA/Goddard Space Flight Center, Code 910.3, Greenbelt, MD 20771.

with a half-width of about 600–700 km. Bonner found that synoptic conditions most favorable for jet formation are a strong pressure gradient across the Great Plains with northward flow from the Gulf of Mexico. Bonner and Paegle (1970) documented further the diurnal cycle in the low-level wind at Ft. Worth, Texas, from 11 years of data.

Several mechanisms have been proposed to account for the strength, direction, and diurnal and seasonal variability of the low-level winds in this region. Wexler (1961) suggested that the LLJ is the result of a northward turning of the trade winds as they encounter the Rocky Mountains. Blackadar (1957) explained the formation and turning of the nocturnal jet as an inertial oscillation that occurs after the daytime turbulence in the planetary boundary layer is attenuated. Bleeker and Andre (1951) suggested that LLJ forms as a result of a large-scale drainage wind caused by nighttime radiational cooling along the slopes of the Rocky and Appalachian Mountains. Holton (1967) studied LLJs in a thermal-viscous boundary layer model and concluded that while thermal forcing may be important, the timing of the jet was not consistent with this mechanism. Instead, he pointed out the importance of the diurnal variability of the eddy viscosity and heat diffusion coefficients in the lower troposphere. Bonner and Paegle (1970) investigated the influence on low-level winds of the diurnal cycle of heating on sloped terrain just east of the Rocky Mountains. They found that the resultant oscillation in the geostrophic wind was of significant magnitude but of the wrong sign to explain the observed oscillation in the boundary layer winds. Paegle et al. (1984) suggested that increased nighttime stratification might initiate a topographic flow-blocking mechanism to produce an LLJ.

The location of the jet in the lowest kilometer of the atmosphere suggests it is an important component of the atmospheric moisture budget in this region. Several authors, including Means (1952), Pitchford and London (1962), Wallace (1975), and Astling et al. (1985) have examined the connection between the jet and nocturnal rainfall. The pioneering work of Benton and Estoque (1954) and Rasmusson (1967) provided clear observational evidence for the key role of the mean jet in bringing Gulf Coast moisture into the continental United States; the latter study also showed a significant diurnal signal in the moisture fluxes. On the other hand, the small vertical extent and diurnal nature of the jet have made it difficult to study the detailed nature of the jet and its role in the continental-scale moisture budget from observations alone. For example, Rasmusson (1968) demonstrated the limitations of the observational network for determining accurate moisture budgets, particularly for regions significantly smaller than the continental United States.

The current study is a preliminary investigation of the LLJ and its representation in the Goddard Earth Observing System (GEOS-1) Atmospheric General Circulation Model (AGCM). We will first establish the validity of the GEOS-1 AGCM as a tool for carrying out such an investigation by comparing the model-simulated climatology of the LLJ with the observed climatology. We will then attempt to extend our knowledge of the climatology of the LLJ through analysis of the model simulation, and we will make some general speculations on the interpretation and cause of the LLJ that will be subject to confirmation through future integrations with the AGCM. Finally, we shall discuss the role of the simulated LLJ in the moisture budget of the continental United States.

While several regional boundary layer models (Astling et al. 1985; Krishna 1968; McCorcle 1988; Paegle and McLawhorn 1983; McNider and Pielke 1981; Fast and McCorcle 1990) have been successful in simulating aspects of the jet, the extent to which the jet is resolved in global AGCMs has not yet been documented in the literature. A realistic simulation of the LLJ in a global model has the obvious advantage that it allows studies of how the jet interacts with the large-scale flow. Resolution of the jet also has important implications for the role of the GEOS-1 AGCM as a key component of the GEOS data assimilation system (Schubert et al. 1993), since most of the low-level information provided by that system is dynamically interpolated by the prognostic model between the available data. Thus, it is necessary for the assimilating AGCM to have the proper regional climate statistics when attempting to resolve a spatially and temporally confined phenomena such as the LLJ from observations. Data assimilation offers one of the best means of determining the atmosphere's moisture and wind fields at the resolution and accuracy necessary for computing moisture budgets.

Section 2 describes the formulation of the GEOS-1 AGCM, with particular emphasis on that of the planetary boundary layer, and the details of the integration that has been carried out with the GEOS-1 AGCM for this study. The structure, climatology, and diurnal cycle of the simulated jet are discussed in section 3. The associated moisture transport and the role of the jet in the moisture budget over the continental United States are presented in section 4. A summary and discussion are given in section 5.

2. The integration with the GEOS AGCM

a. Formulation of the hydrodynamics and physics

The GEOS-1 AGCM employs a potential enstrophy and energy-conserving horizontal differencing scheme on a C grid developed by Sadourney (1975) and further described by Burridge and Haseler (1977). An eighth-order Shapiro filter is applied to the wind, potential temperature, and specific humidity to avoid nonlinear computational instability. The filter is applied at every

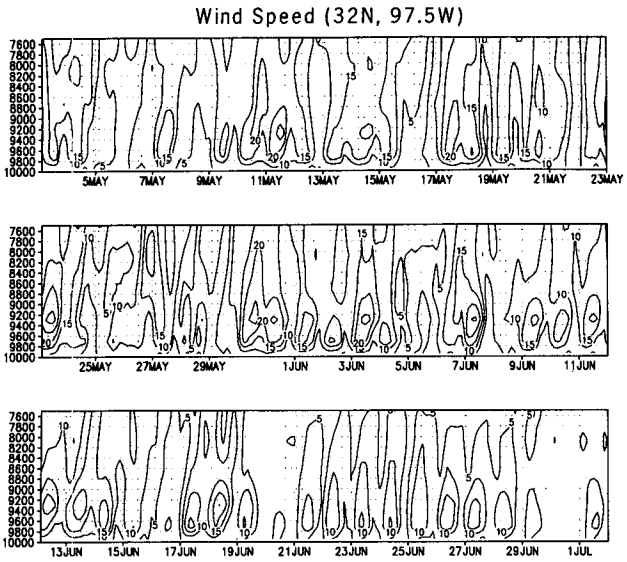

FIG. 1. Vertical profile of wind speed sampled every three hours for the two-month (May–June) model simulation at the grid point closest to Ft. Worth, Texas (32°N, 97.5°W). The pressure levels (mb × 10) are approximated assuming a surface pressure of 1000 mb.

step in such a way that the amplitude of the two-grid interval wave would be reduced to 1/4 its value in two hours, while the three- and four-grid interval waves retain about 2/3 and 11/12 of their respective values over that interval of time. The model also uses a high-latitude Fourier filter to avoid linear instability due to violation of the Courant–Friedrichs–Lewy (CFL) condition for the Lamb wave and internal gravity waves. This polar filter, however, is applied only to the tendencies of the winds, potential temperature, specific humidity, and surface pressure. The model's vertical finite differencing scheme is that of Arakawa and Suarez (1983). The aforementioned dynamics routines are organized into a plug-compatible module called the ARIES/GEOS "dynamical core" (Suarez and Takacs 1993). The model is generally run with a horizontal resolution of 2° lat × 2.5° long with 20 sigma pressure levels in the vertical extending from the surface up to 10 mb, but it can also be run with 1° × 1.25° or 4° × 5° horizontal resolution or with 46 levels in the vertical extending up to 0.1 mb. The lowest five layers of the atmosphere are centered at sigma values of 0.994, 0.971, 0.930, 0.874, and 0.808, which roughly correspond to elevations above the ground of 50, 250, 600, 1100, and 1700 m, respectively.

The infrared and solar radiation parameterizations follow closely those described by Harshvardhan et al. (1987). Absorption bands for longwave radiation are parameterized as in Chou (1984) for water vapor, as in Chou and Peng (1983) for the 15-μm band for CO_2, and as in Rodgers (1968) with modifications by Rosenfield et al. (1987) for ozone. The shortwave follows Davies (1982), as described in Harshvardhan et al. (1987). Shortwave absorption by water vapor uses a k-distribution approach as in Lacis and Hansen (1974). Cloud albedo and transmissivity for the model layers are obtained from specified single-scattering albedo and cloud optical thickness using the delta-Eddington approximation (Joseph et al. 1976; King and Harshvardhan 1986).

The penetrative convection originating in the boundary layer is parameterized using the relaxed Arakawa–Schubert (RAS) scheme (Moorthi and Suarez 1992), which is a simple and efficient implementation of the Arakawa–Schubert (1974) scheme. Unlike the Arakawa–Schubert scheme, which solves an adjustment problem by considering simultaneous interaction among all possible cloud types, RAS considers only one cloud at a time, and rather than adjusting fully every hour or two, it does a series of partial adjustments that tend to relax the state toward equilibrium. The AGCM also includes a parameterization that models the evaporation of falling convective rain as described in Sud and Molod (1988). Negative values of specific humidity produced by the finite-differenced advection are filled by borrowing from below.

b. *The planetary boundary layer formulation*

The vertical structure of the planetary boundary layer (PBL) is explicitly resolved in the GEOS-1 AGCM into a region of several model layers, which should approximate the physical depth of the PBL. A 100-mb-deep PBL, for example, would consist of four model layers. The lowest layer of the AGCM corresponds to an atmospheric surface layer for which wind, temperature, and humidity profiles and the turbulent surface fluxes of heat, moisture, and momentum are obtained from the Monin–Obukov similarity theory. The similarity functions (Eqs. (A1), (A2), (A4), and (A5) of the appendix) have been chosen, as in Helfand (1985), to approach the convective limit for unstable profiles and to agree with observations for very stable profiles. Turbulent roughness lengths over land surfaces are taken as functions of vegetation type, as prescribed by the Simple Biosphere dataset of Sellers et al. (1986), and as a function of surface stress over water surfaces, as described in the appendix. There is also a parameterization of the viscous sublayer [Eq. (A7) of the appendix] based on the work of Yaglom and Kader (1974), which takes into account temperature and moisture gradients that can be quite large in the essentially laminar region between the earth's surface and the tops of the roughness elements.

Turbulent vertical fluxes of momentum, heat, and moisture in the region of the PBL above the surface layer or in disjoint layers of turbulence above the PBL are predicted above the surface layer by the level 2.5, second-order turbulence closure scheme of Helfand and

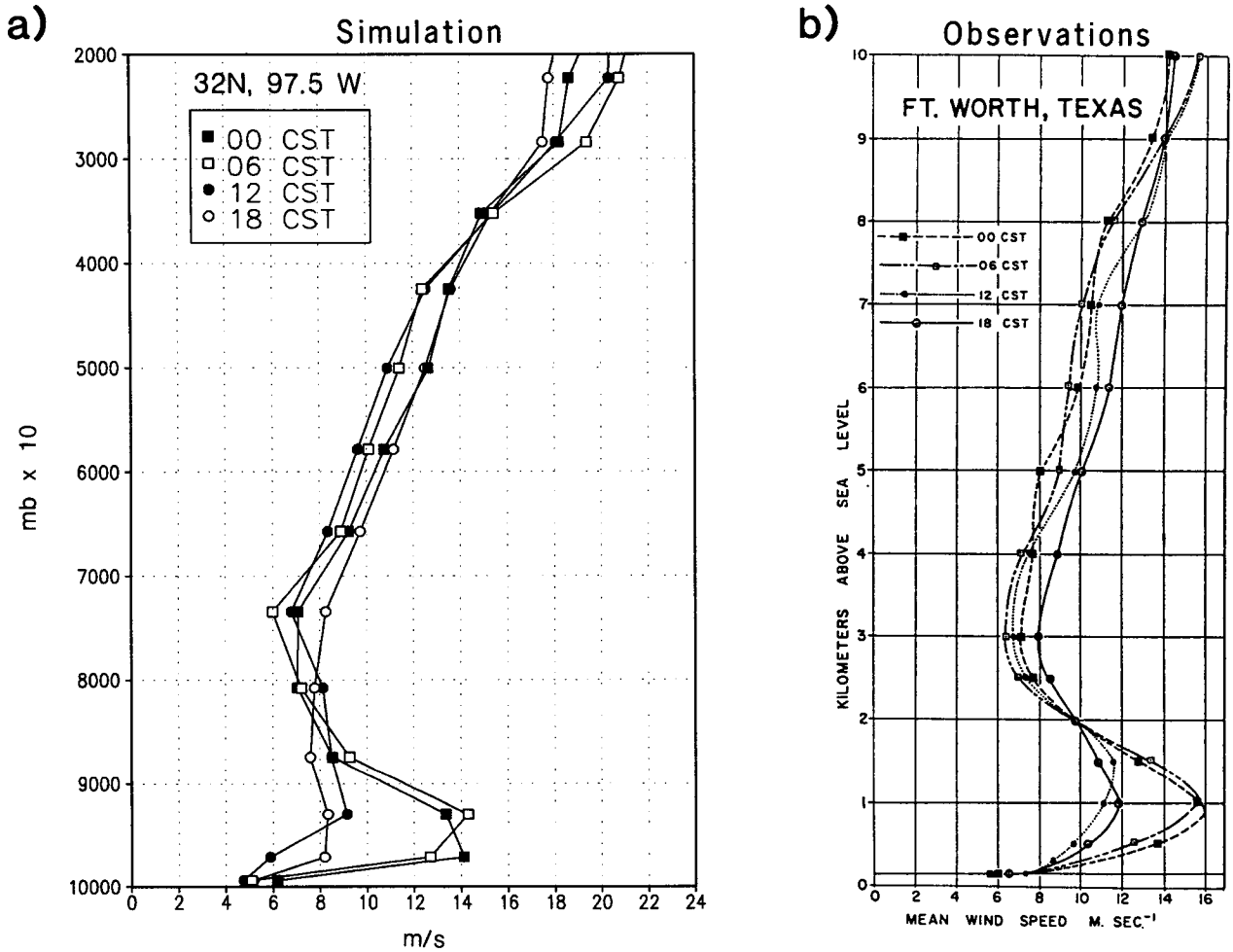

FIG. 2. Vertical profile of the time-averaged wind speed at the four synoptic times (a) for the summer period (1 June–2 July) of the model simulation at the grid point closest to Ft. Worth, Texas (32°N, 97.5°W), and (b) for the observations at Ft. Worth, Texas, for 16 summer "jet days" (taken from Bonner 1968). For (a), the pressure levels (mb × 10) are approximated assuming a surface pressure of 1000 mb.

Labraga (1988), which is a statistically realizable version of the level 2.5 scheme of Yamada (1977). This scheme predicts turbulent kinetic energy (TKE) as a prognostic variable and the remaining second turbulent moments, including vertical fluxes, as diagnostic variables. It uses an implicit backward operator to determine the turbulent diffusion of TKE and of the first moments, but uses a time-forward computation to determine the rate of production of TKE. Within the PBL, the turbulent length scale ℓ, Eq. (A8), increases with increasing depth of the PBL, but the formulation also applies to disjoint, elevated layers of turbulence, Eqs. (A8) and (A10), even when those layers are statically stable.

c. *The simulation*

The GEOS-1 AGCM has been integrated for two months at a resolution of 2° latitude by 2.5° longitude with 20 sigma pressure levels in the vertical. These include five levels below 800 mb and seven levels above 200 mb. The simulation was initiated from data from a GEOS assimilation for 0300 UTC 3 May 1988 and integrated until 0300 UTC 2 July 1988. Boundary conditions have been taken from climatology; both the soil moisture and sea surface temperature boundary conditions are seasonally varying monthly averages computed from the years 1979–89. The soil moisture computation has been carried out off-line with a simple bucket model from monthly mean observed surface air temperature and precipitation data (Schemm et al. 1992).

All fields have been saved every three simulated hours at the model sigma levels to minimize both the errors and the loss of information introduced by interpolation and sampling. This is particularly important for resolving the low-level jet, which is confined

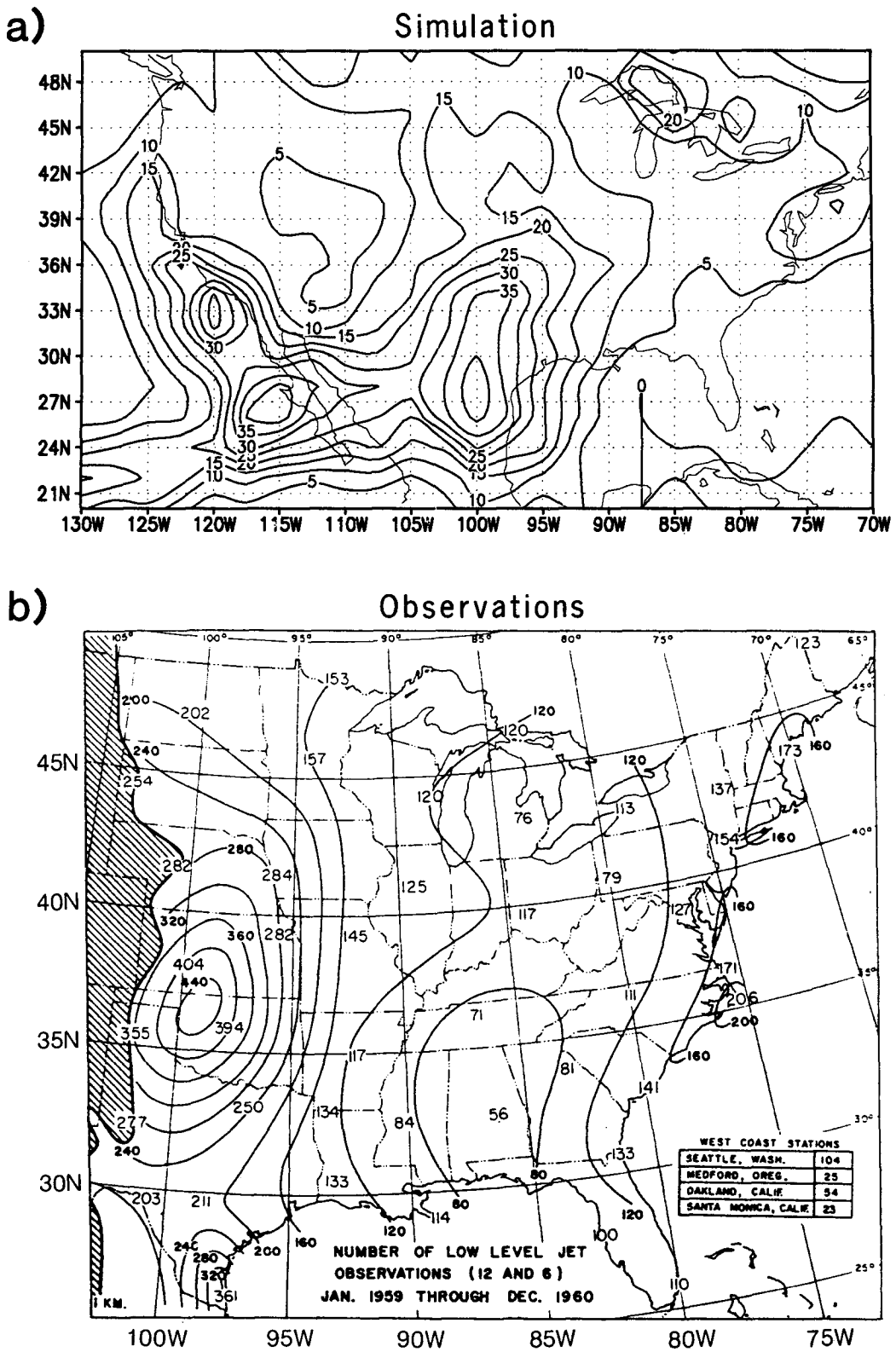

FIG. 3. Frequency of criteria 1 jets for (a) the two-month (May–June) model simulation and (b) two years of observations (taken from Bonner 1968). For the observations, divide by 1462 (the maximum possible number of observations) to obtain percentages.

to the lowest kilometer and has a strong diurnal component.

3. Simulation of the low-level jet

a. Vertical and temporal structure

The simulated low-level jet is evident in the time series of wind speed (Fig. 1) for the grid point closest to Ft. Worth, Texas, (32°N, 97.5°W) as a low-level, quasi-regular, nocturnal peak of 10–25 m s^{-1}, which occurs from 30 to 70 mb (roughly 250–600 m) above the earth's surface. These nocturnal winds are predominantly from the southerly direction. The mean diurnal cycle of wind speed for this grid point has been obtained for the summer period of the integration by averaging together all of the diurnal cycles for the period 1 June–2 July (Fig. 2a). A wind-speed maximum of about 14 m s^{-1} develops at about 30 mb (roughly 250 m) above the surface by 0000 CST (Central Standard Time). It persists through the early morning, rising slightly in elevation to about 70 mb (roughly 600 m) above the surface by 0600 CST, until enhanced surface friction associated with a thermally unstable daytime surface layer retards the boundary-layer wind by 1200 CST. The boundary-layer wind becomes well mixed due to thermally driven turbulence by 1800 CST and the jet maximum does not redevelop until 0000 CST of the following day. This simulated behavior shows a remarkable agreement with Bonner's (1968) observations (Fig. 2b) for a period of 16 summer days at Ft. Worth, Texas, during which the jet was active. There is agreement, even for more subtle features such as the reversal of the wind-speed trend at about 170 mb above the surface. The extension of the diurnal signal into the middle troposphere will be discussed further in section 3d.

b. Climatology of LLJ frequency

Bonner (1968) examined the spatial and temporal characteristics of the LLJ by using three progressively more stringent criteria to identify the presence of an LLJ from the vertical sounding of wind speed. His criteria 1, 2, and 3 specify that the wind-speed profile have a maximum of at least 12, 16, or 20 m s^{-1}, respectively, within 1.5 km of the ground, and that the wind-speed decrease by at least 6, 8, or 10 m s^{-1}, re-

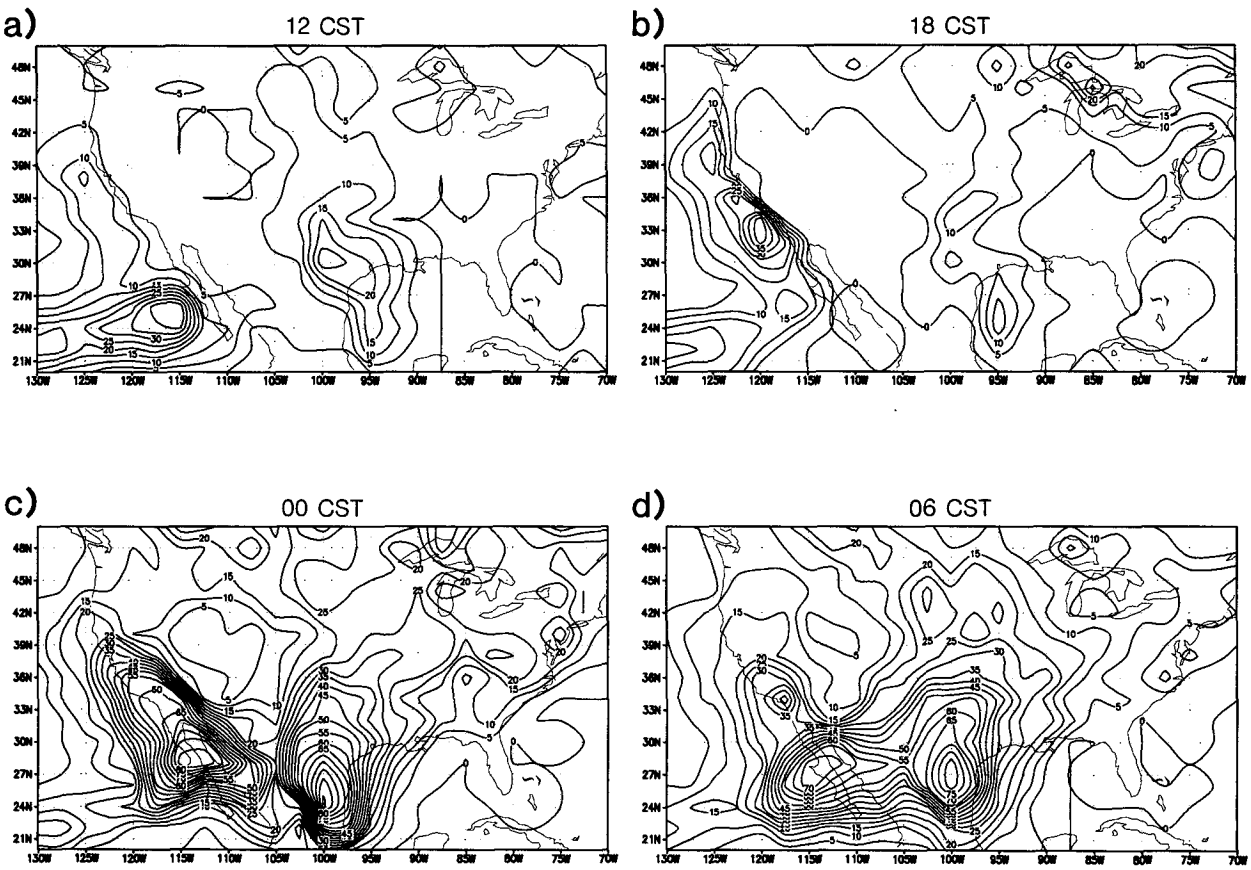

FIG. 4. Frequency of criteria 1 jets for the two-month (May–June) model simulation as a function of synoptic time.

spectively, at the lowest minimum located above the maximum at or below the 3-km level.

The simulated climatology for frequency of occurrence of the LLJ has been computed according to each of these three criteria for the synoptic observation times, 0000 and 1200 UTC (1800 and 0600 CST), during the two-month period of integration, but only the criterion 1 frequencies are shown here (Fig. 3a). By way of comparison, the observed climatology of criterion 1 frequency for the 2-yr period January 1959–December 1960 is shown in Fig. 3b (after Bonner 1968). Percentage frequency may be obtained from Fig. 3b by dividing the number of occurrences by the total number of observed profiles (1462).

The simulated structure of LLJ frequency over the eastern half of the United States is quite similar to that observed by Bonner despite the disparity in the averaging periods. LLJ frequency maxima are aligned in both the simulation and the observations along an axis that runs from the Gulf Coast of Texas and Mexico to central Texas and then north-northeastward toward Iowa and Minnesota. Quantitatively, the peak frequencies are reasonably close with a maximum of about 40% in the simulation and of about 30% in the Bonner climatology. However, the Bonner climatology exhibits a double maximum, one near the Oklahoma–Kansas border and a second near Brownsville, Texas (which is artificially cut off at the Mexican border or the southern limit of the region of analysis), while the simulation exhibits a single elongated peak in southern Texas (not far from Brownsville) with only the hint of a second maximum near the Texas–Oklahoma border (slightly south of the observed inland maximum). Comparison is similar between the simulated and observed frequency maps for both criterion 2 and 3 (not shown) except that the simulated frequencies do not decrease as rapidly with increasingly stringent criterion in the simulation as they do in the observations.

These differences between the simulation and the observations might be due to the different averaging periods for the two studies. The higher jet frequencies of the simulation would surely become lower if the integration were extended to include the more quies-

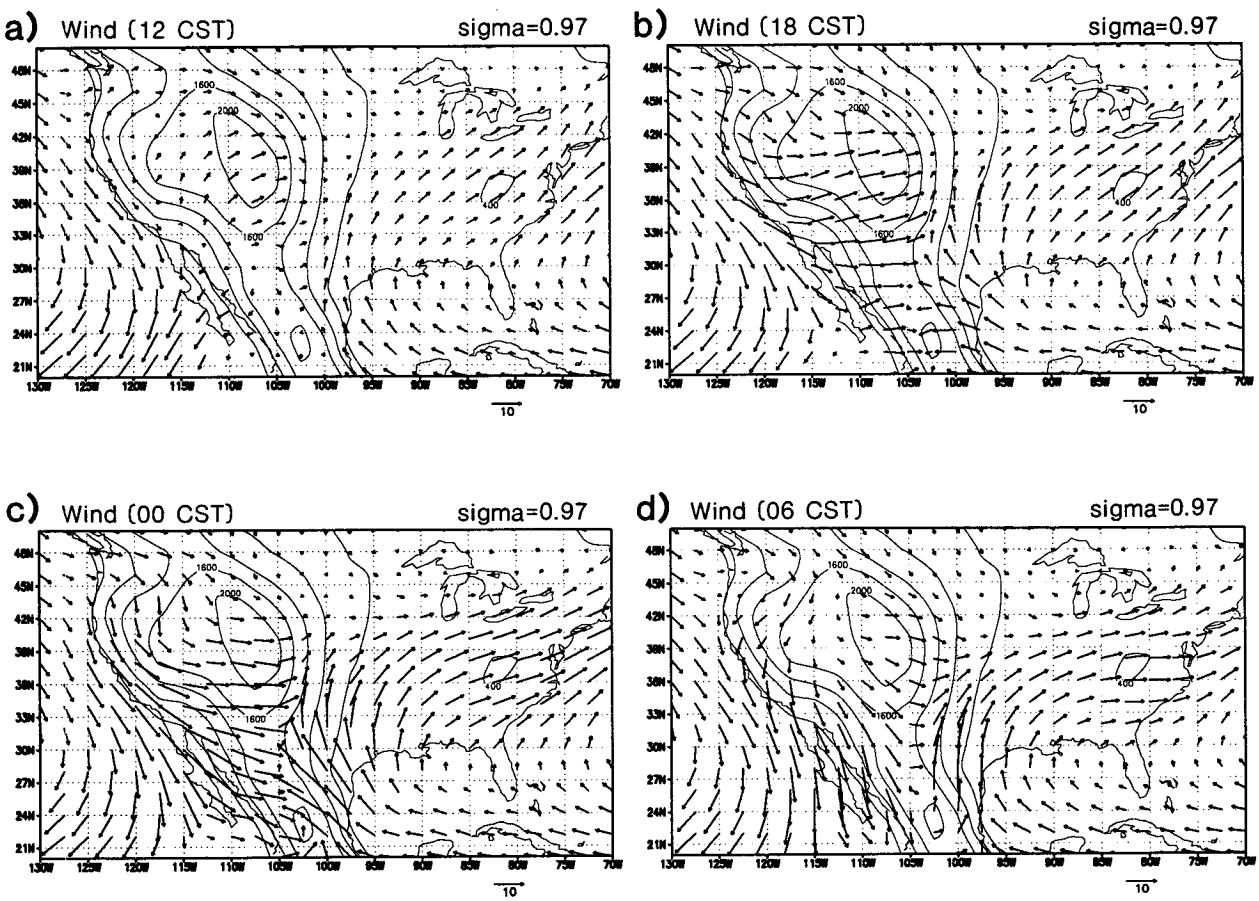

FIG. 5. Wind vectors at the second sigma level (σ = .97) for the two-month (May–June) model simulation at the four synoptic times. Units are m s^{-1}. The contours denote the surface height. Contour interval is 400 m.

cent late fall, winter, and early spring periods. Also, a week-by-week series of criterion 1 frequency maps shows a predominant frequency maximum that fluctuates in position about Brownsville, Texas, during the month of May and then weakens in June. A second, inland maximum strengthens during the month of June and appears to move northward and eastward toward the end of the month. The two maxima of the 2-yr average shown in Fig. 3b could correspond to the superposition of an early springtime maximum near Brownsville and a middle-to-late-summer inland maximum that has not been fully captured during the period of integration. Analysis of a longer multiyear simulation with the GEOS-1 AGCM is currently under way to investigate these possibilities.

An additional double maximum of LLJ frequency appears in the simulation off the Pacific coasts of California, at 33°N, and Baja California, at 27°N. This region is not examined in the Bonner analysis, but there may be some observational evidence for the existence of these maritime LLJ maxima. The U.S. Navy *Marine Climatic Atlas of the World* (U.S. Navy 1956) shows frequency maxima of surface winds in excess of 10 kt off the California coast at 32°N, 122°W for May (Chart 54), and off the Baja California coast at 28°N, 115°W for June (Chart 66), corresponding well with the two maxima of the simulation.

c. *The diurnal cycle of the LLJ*

The simulated LLJ exhibits a strong diurnal oscillation (Fig. 4) over land surfaces. Its frequency increases dramatically over the southern Great Plains of the United States and northeastern Mexico from a few percent at 1800 CST (0000 UTC) to values greater than 80% over southern Texas and as large as 95% over northeastern Mexico by 0000 CST (0600 UTC). Its frequency increases from a few percent to values greater than 80% over Baja California during the same time period. The LLJ frequency decreases over northeastern Mexico and Baja through the early morning while it grows over the southern Great Plains during this time. LLJ frequency then decreases dramatically over all land regions by 1200 CST (1800 UTC) and throughout the rest of the afternoon. The diurnal cycle over the Pacific Ocean and the Gulf of Mexico is much weaker than it is over land surfaces.

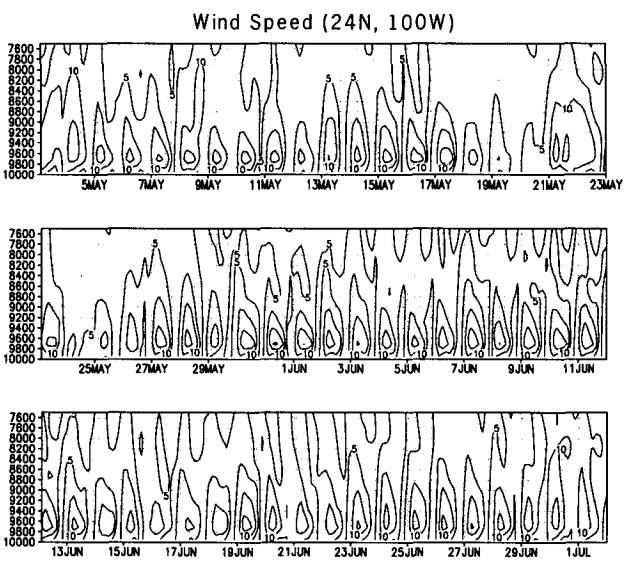

FIG. 6. Vertical profile of wind speed sampled every three hours for the two-month (May–June) model simulation at 24°N, 100°W. The pressure levels (mb × 10) are approximated assuming a surface pressure of 1000 mb.

The diurnal cycle of the simulated wind vectors at the $\sigma = .97$ level (about 250 m above the surface) in the boundary layer, shown in Fig. 5 together with contours of the surface elevation, is strikingly coherent and regular on the subcontinental scale. Over the southern Great Plains between 1200 and 1800 UTC, there is a significant southerly acceleration of the low-level winds parallel to the eastern contours of the Rocky Mountains. As one moves southward along the Gulf Coast into Mexico, the low-level acceleration gradually becomes easterly and upslope. This east Mexican easterly LLJ represents the direct westward penetration of the anticyclonic, subtropical Atlantic gyre (associated with the Bermuda High) from the Gulf of Mexico into the North American continent, while the Great Plains jet consists of a deeper, northwestward and then northeastward, extratropical penetration of the gyre into the interior of the continent where it is subject to much synoptic-scale variability. Thus, the east Mexican LLJ (Fig. 6) is a much more regular and predictable feature of the diurnal cycle of the Atlantic gyre than is the Great Plains southerly LLJ (Fig. 1).

The California jets are features of an anticyclonic, subtropical east Pacific gyre that has little diurnal variability over the open ocean. However, there is a marked diurnal cycle just off the coasts of California and Baja California where the northwesterly flow accelerates throughout the late afternoon and evening and eventually rotates to become northerly flow. There is an even stronger diurnal signal in the region between the two gyres, that is, over the continent west of about 105°W, where the PBL winds are weak during the day, accelerate to strong westerlies (northwesterlies over Baja California) between 1800 and 0000 CST, turn anticyclonically through the night, and are again decelerated by surface friction by 1200 CST.

At the $\sigma = .87$ level (approximately 1100 m above the surface) in the free atmosphere the diurnal variability is greatly reduced (Fig. 7). Both the Atlantic and the east Pacific subtropical gyres are present at this level. The Atlantic gyre is tighter than it is in the

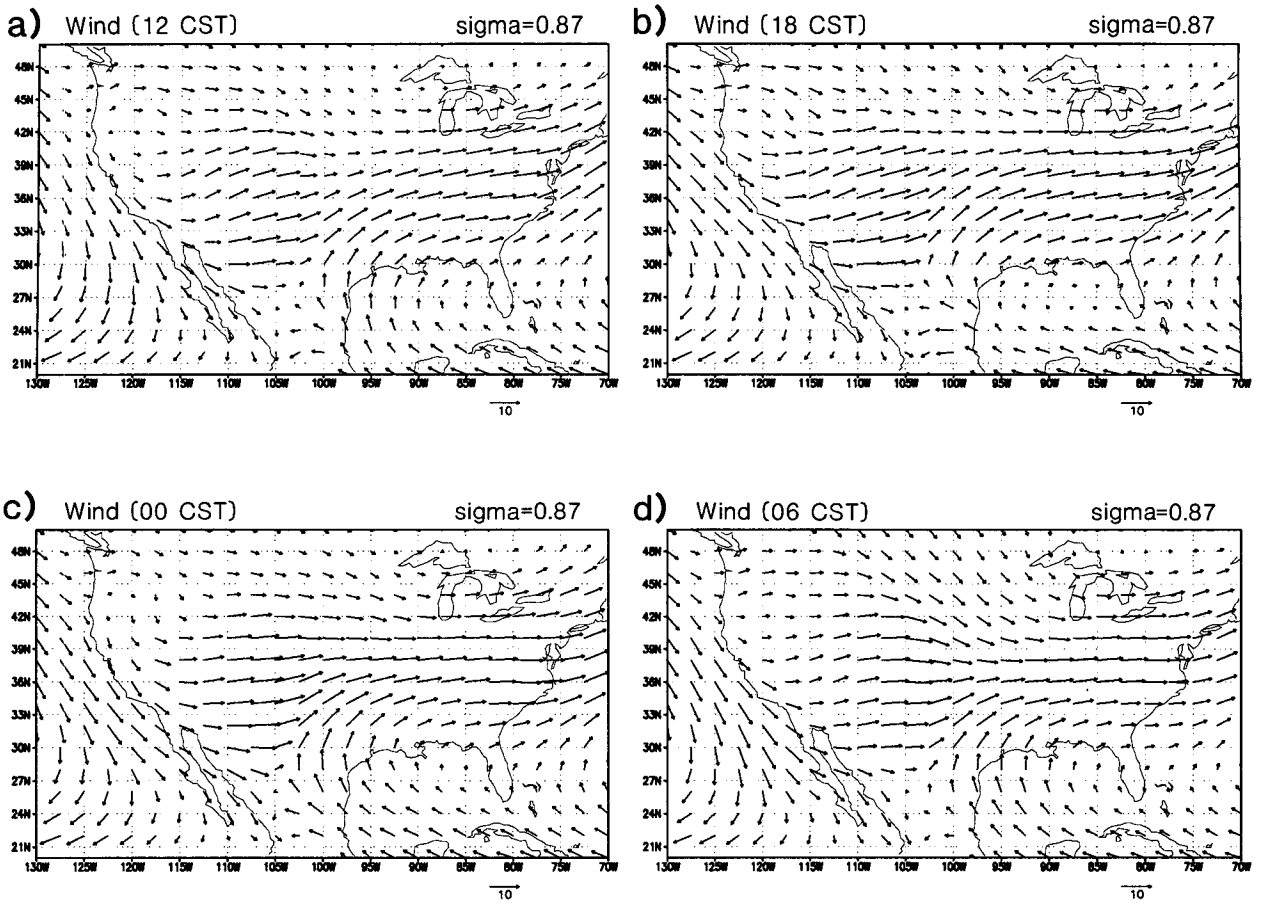

FIG. 7. Wind vectors at the fourth sigma level (σ = .87) for the two-month (May–June) model simulation at the four synoptic times. Units are m s^{-1}.

boundary layer with reduced westward penetration into the Mexican plateau and less northward penetration into the Great Plains of the United States. This is due, perhaps, in part to the lack of surface friction in the free atmosphere and in part to the baroclinic structure of the subtropical atmosphere. It is the contrast of the southerly nocturnal winds in the boundary layer with the free atmospheric westerlies that gives rise to the LLJ structure. The configuration of the east Pacific subtropical gyre in the free atmosphere is similar to that in the PBL but weaker so that the wind-speed maxima for the two California LLJs are indeed located within the PBL region. The flow across the U.S. Rocky Mountains in the free atmosphere is westerly and nearly constant in time, in contrast to the quiescent daytime boundary layer flow in this region that accelerates to match the free atmospheric flow by 1800 CST after daytime surface friction has died down, and then rotates anticyclonically until it is once again weakened by daytime surface friction. A further discussion of the vertical structure of the diurnal signal is given in the next section.

Figure 8 summarizes the anticyclonic rotation and the nighttime strengthening of the wind vectors over Mexico and the southwestern United States during the

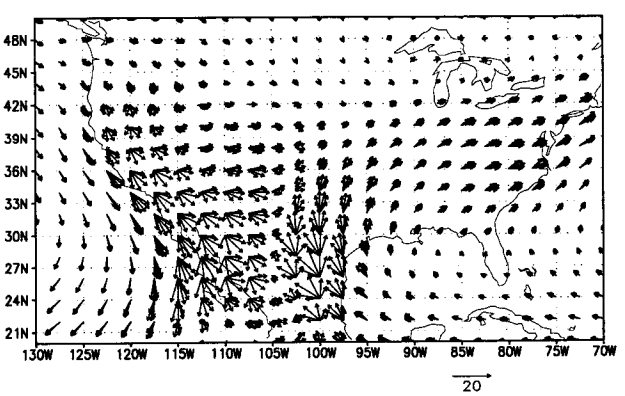

FIG. 8. Diurnal rotation of the wind vectors at the second sigma level (σ = .97) for the two-month (May–June) model simulation at 1800, 2100, 0000, 0300, 0600, and 0900 CST. Vectors rotate clockwise. Units are m s^{-1}.

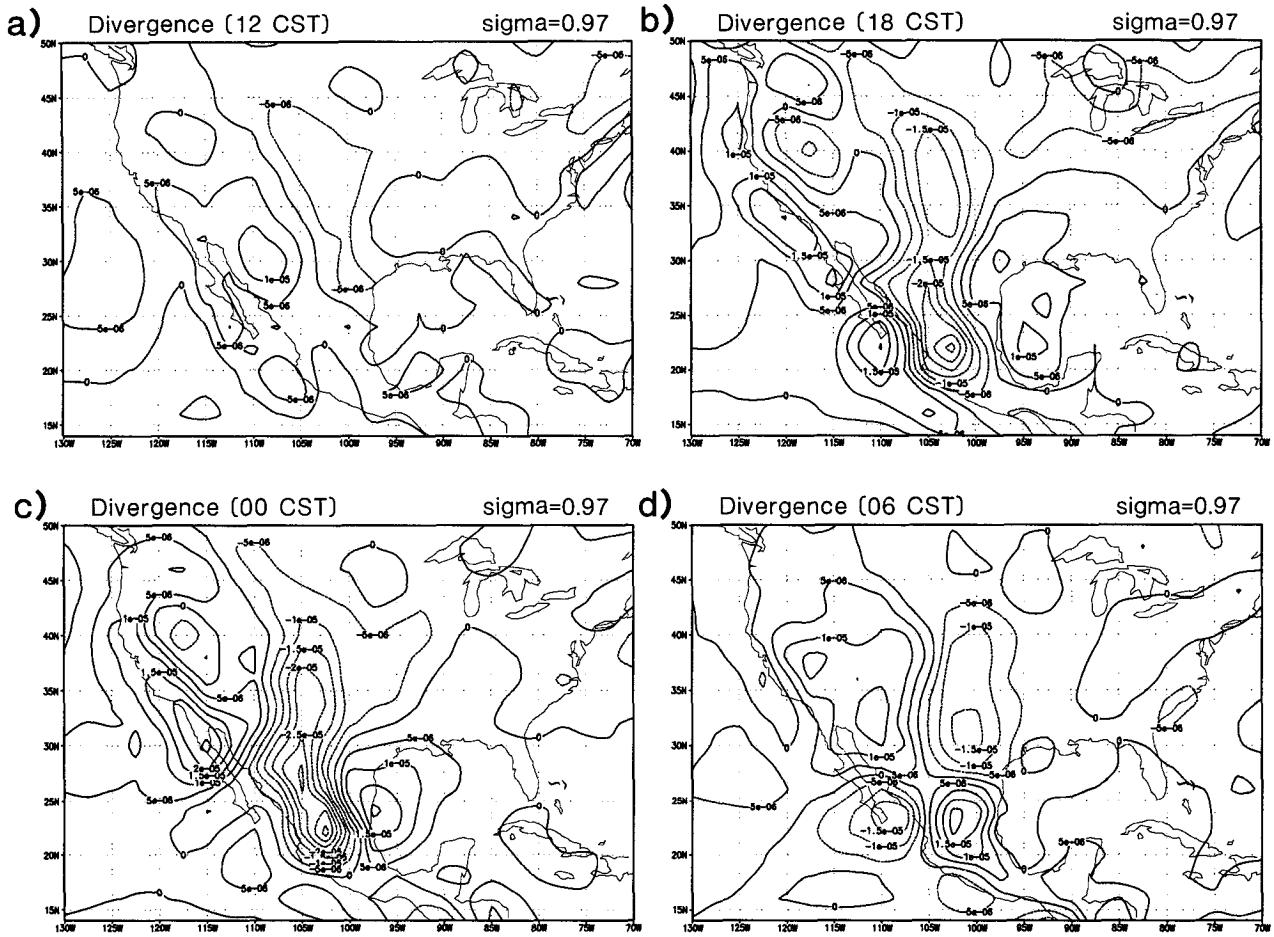

FIG. 9. Divergence (computed on the sigma surface) at the second level (σ = .97) for the two-month (May–June) model simulation at the four synoptic times. Units are s^{-1}.

period 1800–0900 CST. This is consistent with the idea that the LLJ is an inertial oscillation that is initiated by an Ekman imbalance due to the sudden decline over land surfaces of daytime turbulence. Note that there is little diurnal change of the wind over the open Pacific Ocean and Gulf of Mexico.

The simultaneous acceleration of the low-level easterlies and southerlies of the Atlantic gyre and the low-level westerly acceleration over the western United States and Mexico by 1800 CST results in marked low-level convergence (computed on the sigma surface) over the eastern slopes of the U.S. Rockies and over the Mexican High Plateau (Fig. 9), with enhanced divergence in the Gulf of Mexico and off the Pacific coast of the United States and Mexico. These accelerations, convergences, and divergences are further enhanced by 0000 CST, except near the southern tip of Baja California. There is little change in wind speed between 0000 and 0600 CST, but additional anticyclonic turning of wind direction results in a half-wave east–west phase shift of the divergence pattern over central Mexico and a weakening of the convergence over the Great Plains. By 1200 CST, the low-level winds and divergence pattern over land surfaces virtually disappears.

The diurnal trends in the boundary layer at or near land surfaces might be attributed to diurnal changes in the land–sea contrast of surface heating or surface friction, to periodic changes in the geostrophic wind, to periodic changes in convergence patterns associated with the elevated heat source of inland mountains, or to the rapid increase and decrease of surface friction as the lapse rate near the ground changes. We hope to shed light on these hypotheses in the near future by carrying out sensitivity integrations with the GEOS AGCM.

d. The diurnal cycle of the middle- and upper-level flow

While the diurnal signal over much of the United States and northern Mexico is strongest at low levels,

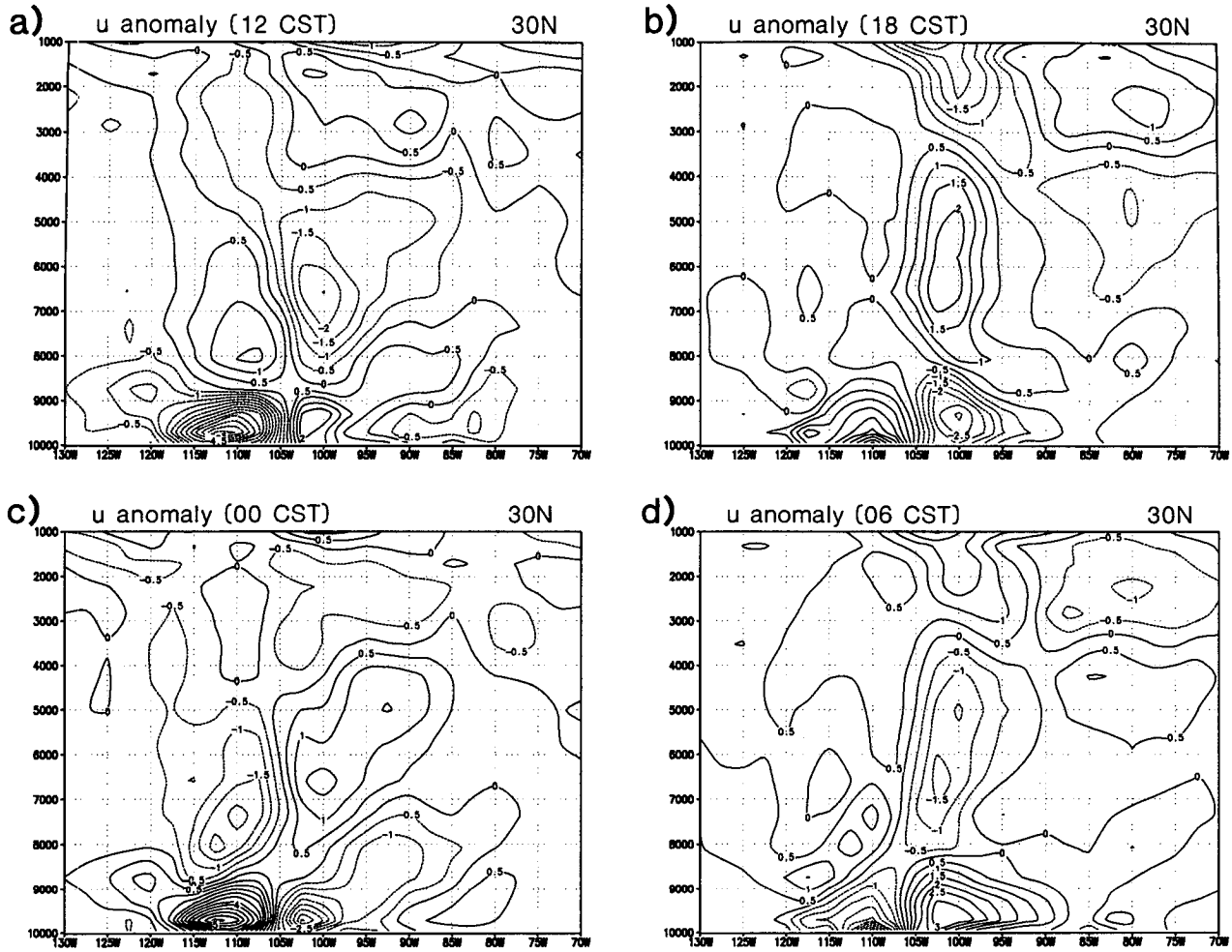

FIG. 10. Cross section of zonal wind anomaly (deviation from time mean) at 30°N for (a) 1200 CST, (b) 1800 CST, (c) 0000 CST, and (d) 0600 CST. Pressure levels are approximate assuming a surface pressure of 1000 mb. Units are m s^{-1}.

it also extends, in some regions, well into the middle and upper troposphere. Hering and Borden (1962) were the first to find observational evidence for diurnal cycles in the middle and upper level winds when they examined summertime wind profiles over Ft. Worth, Texas, and Shreveport, Louisiana. The station data in that study showed maximum amplitudes of the diurnal signals of wind speed at about 0.6, 5, and 12 km, which tended to be out of phase with each another (see their Figs. 1 and 2).

Such phase reversals in the diurnal signal are also evident in the simulation, as can be discerned from Fig. 2a and can be seen more readily in Figs. 10 and 11, which show cross sections at 30°N of the simulated anomalous (deviations from the time mean) zonal and meridional winds, respectively, at the four synoptic times. The out-of-phase relationship between the lower- and middle-level wind anomalies is evident on both slopes of the Rocky Mountains, and an upper tropospheric–lower stratospheric signal is also discernible on the eastern slope (east of 105°W).

The zonal signal in the PBL region is characterized, as we have already seen in Figs. 5 and 9, by a strongly enhanced (cf. Figs. 12a,c) upslope convergence during the late afternoon and evening, followed by an early morning anomalous downslope divergence that lasts well into the next afternoon. The meridional signal, which is dominated by the nocturnal acceleration and daytime deceleration of the Great Plains southerly LLJ and the nocturnal continental incursion of the northerly Baja jet, fits the picture of a clockwise inertial rotation of the low-level winds, as has already been seen in Fig. 8.

There is a reversal of the zonal flow at middle levels with divergence in the zonal wind over the Rockies during the late afternoon and evening followed by early morning convergence, but it is of less intensity and of broader vertical extent than in the PBL. The zonal flow

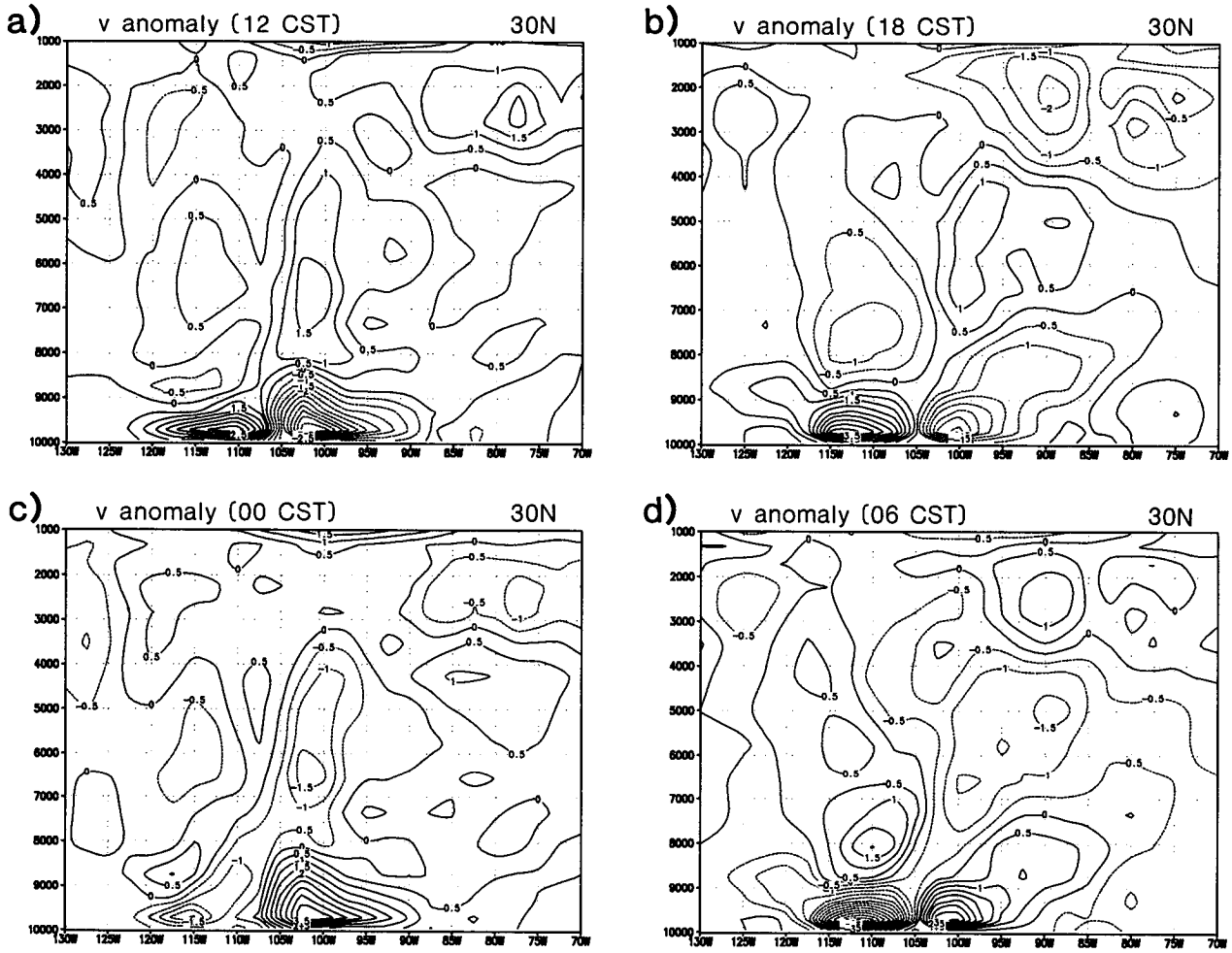

FIG. 11. Same as Fig. 10 except for meridional wind anomaly.

over the Great Plains reverses direction once again near and above the tropopause level to give a pattern of divergence of the same sense as that in the boundary layer. This appears to be an example of a "thermal chimney" in which daytime heating over the high terrain eventually produces inflow at low levels and outflow in the middle levels, which in turn induces inflow aloft; the nighttime cooling eventually produces the reverse circulation. In the meridional wind field, there is a broad, middle-level return flow over the Great Plains LLJ and a more complex return flow over the Baja jet, occurring initially as a shallow layer just above the PBL over the open ocean and later broadening vertically and moving inland.

The diurnal signal in the zonal and meridional winds on the eastern slope of the Rocky Mountains (with flow reversals aloft) is very similar in magnitude and timing to the signal found in the observed winds at Ft. Worth, Texas, by Borden and Hering (1962).

e. The low-level climatological mean flow pattern

The two-month time-mean flow pattern at the $\sigma = .97$ level (Fig. 12a) exhibits the same continental penetration by the Atlantic gyre and Great Plains LLJ flow pattern that is seen in the nocturnal phases of the diurnal cycle. Strong southeasterly flow from the Gulf of Mexico turns clockwise to become southerly flow extending deeply into the Great Plains and then southwesterly flow across the eastern United States. This gyre is met abruptly in the lee of the Rockies by a strong westerly flow over the western United States, as in the nocturnal phases. There is a clash between the Atlantic gyre and the west Pacific gyre over the Mexican Plateau too, but it is less abrupt in the time mean than in the nocturnal phases.

The time-mean flow pattern over land surfaces, with its associated zones of strong convergence over the south-central Great Plains and north-central Mexico (Fig. 12c), seems to be more characteristic of an un-

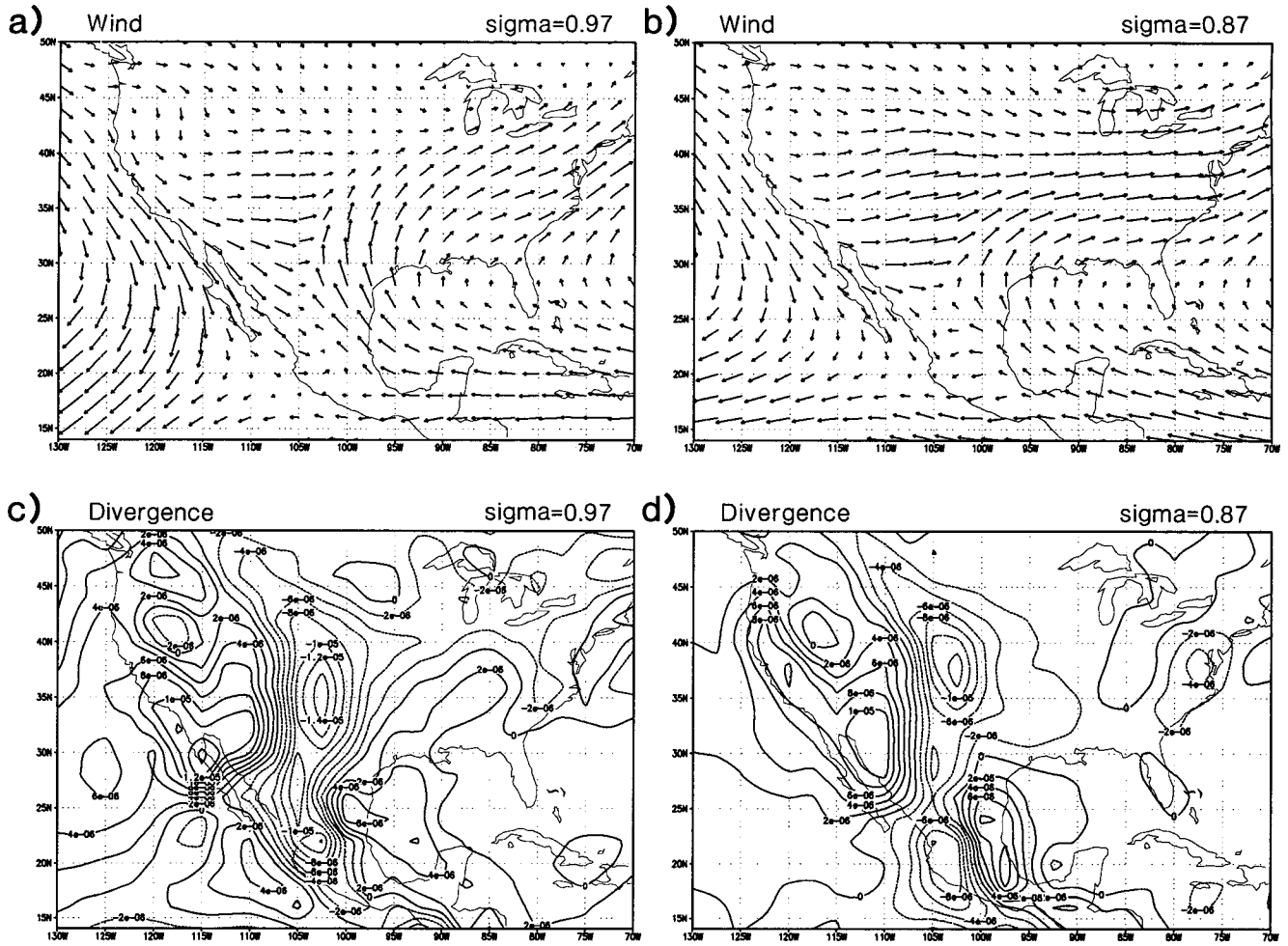

FIG. 12. Wind vectors for the two-month (May–June) model simulation at (a) the second sigma level (σ = .97) and (b) the fourth sigma level (σ = .87). Units are m s^{-1}. Divergence (computed on sigma surfaces) for the two-month (May–June) model simulation at (c) the second level (σ = .97) and (d) the fourth level (σ = .87). Units are s^{-1}.

steady, strongly forced flow than it is of a climatological mean flow. The mean flow pattern over land resembles the nocturnal phase of the diurnal cycle because the low-level daytime winds there are severely weakened by strong surface friction and contribute little to the diurnal average other than to decrease its intensity. Over sea surfaces, surface friction and thermal forcing are fairly constant and the diurnal cycle is relatively weak so that the mean low-level flow away from the edges of the continent is smooth and more reminiscent of a climatological average.

Above the PBL, friction and thermal forcing are weak so there is little diurnal cycle, and the time-mean flow and divergences at the σ = .87 level (Figs. 12b,d) are virtually the same as those for the individual phases of the diurnal cycle. The decrease within the boundary layer of wind speed above the level of its maximum, therefore, is smaller in the time mean than it is in the nocturnal phase because the intensity of the maximum is weaker, with wind speeds often less than 12 m s^{-1}. Thus, the time-mean southerly flow over the southern Great Plains, while it resembles that of the nocturnal LLJ, does not satisfy any of Bonner's three criteria for the existence of an LLJ, and there are no LLJs in the climatological mean flow.

4. Simulation of the moisture budget

a. The role of the LLJ in the moisture budget

The location of the Great Plains jet in the lowest kilometer of the atmosphere and its southerly orientation inland from the Gulf of Mexico suggest that it can be an important source of moisture for the continental United States, as is supported by the observational evidence of Benton and Estoque (1954)

and Rasmusson (1967). The realistic simulation of the LLJ by the GEOS-1 AGCM gives us confidence to use the results of the integration to quantitatively examine the role of the LLJ in the moisture budget for the continental United States. Simulated surface evaporation and precipitation and the simulated atmospheric transport of moisture are available at a frequency of three hours for the two-month period of integration. The moisture transport can be spectrally decomposed into contributions from the time-mean flow and from transients of various frequencies, as is described in section 4b below. The simulated moisture budget over the continental United States is described quantitatively in section 4c.

b. *Temporal decomposition of moisture transport*

The horizontal moisture transport can be decomposed into a time-mean transport and contributions from transients of selected frequencies as follows. The horizontal time-mean moisture flux may be written as

$$\overline{vq} = \bar{v}\bar{q} + \overline{v^*q^*} + \overline{v'q'}, \qquad (1)$$

where q is the specific humidity and v is the horizontal wind vector. The overbar is a time mean for the period starting 2100 CST 3 May and ending 2100 CST 2 July. The deviations from the time mean are further separated into a contribution from the diurnal cycle (denoted by a star) and the remaining transients (denoted by a prime). The diurnal cycle is computed by aver-

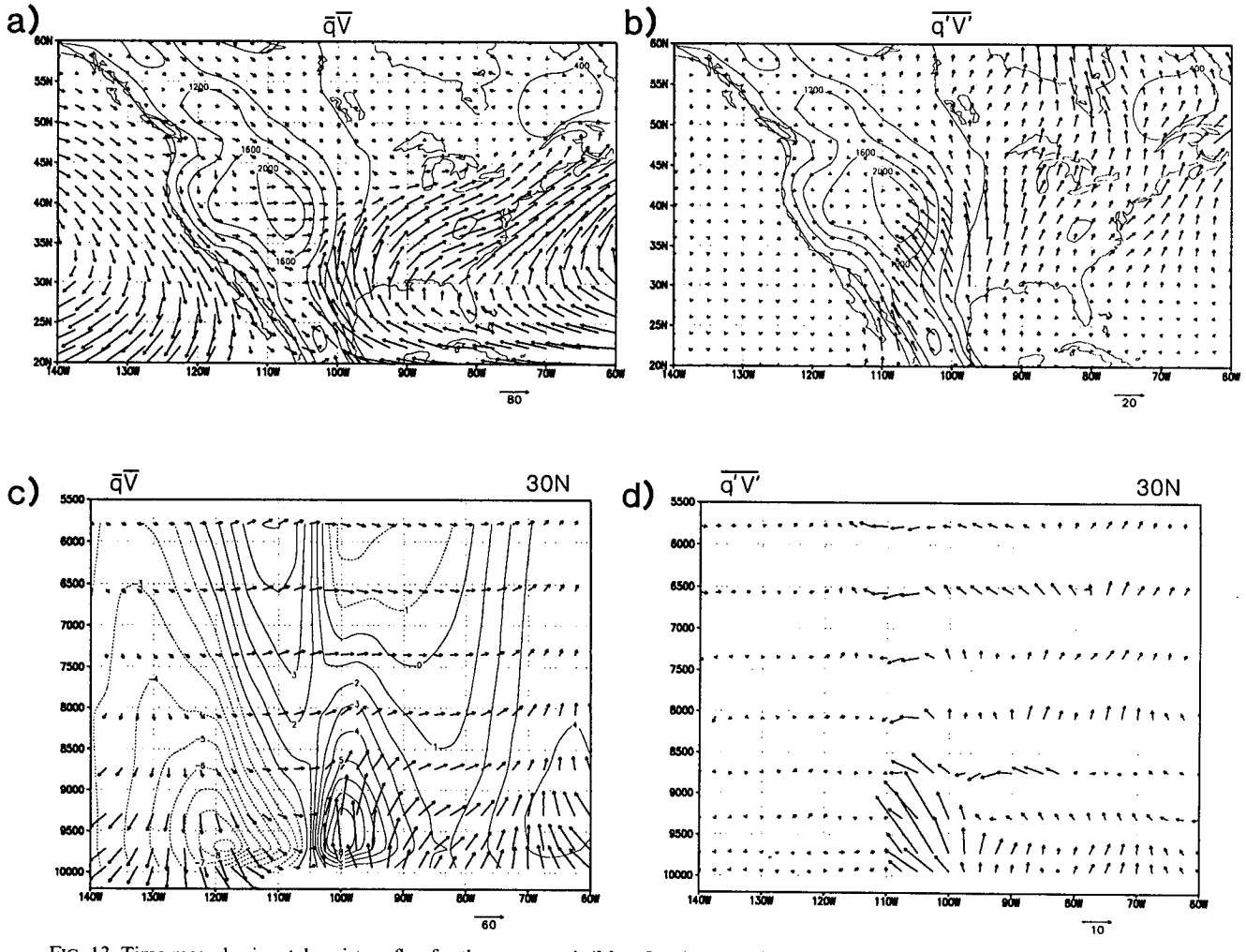

FIG. 13. Time mean horizontal moisture flux for the two-month (May–June) model simulation. Contributions to the mean flux from the time-mean flow and the transients other than the diurnal cycle are shown at the second sigma level (σ = .97) in (a) and (b), respectively. Panels (c) and (d) show the same quantities as (a) and (b) except as cross sections at 30°N (arrows pointing upward denote northward transport). The contours in (c) are of the v wind (units are m s^{-1}). For the cross section plots the pressure levels are computed from the sigma levels assuming a surface pressure of 1000 mb. Units are g kg^{-1} m^{-1}. The maps also show the surface height with a contour interval of 400 m.

aging together all values at 2100 CST, all values at 0000 CST, etc. The first term on the right-hand side of Eq. (1) is the transport associated with the time-mean flow pattern. The second term is the time-mean transport due to the covariance of the diurnal cycle, and the last term is the contribution due to the covariance of transients other than the diurnal cycle.

Figure 13 shows the components of the moisture transport over the continental United States. At the second lowest sigma level (approximately 30 mb above the surface) of the model, the transport associated with the time-mean flow pattern (Fig. 13a) dominates the total transport at this level. Strong southward flux, associated with the large-scale circulation of the east Pacific anticyclone, occurs off the west coast of the United States parallel to the steep topography of the Rocky Mountains. There is very little penetration of moisture flux onto the continent from the west at this level. The greatest flux of moisture into the continent occurs over the Gulf Coast of the United States and Mexico, where it is carried inland by the Atlantic anticyclonic gyre as it appears in the diurnally averaged low-level flow described in the previous sections (Fig. 12a). The magnitude of the flux by the transients other than the diurnal cycle (Fig. 13b) is about a quarter of that by the mean flow. It is largest over the eastern slope of the Rocky Mountains where there is a relatively large upslope flux. The flux by the transients is also relatively large over the central Great Plains and Hudson Bay; in these regions the flux is almost everywhere southerly. The fluxes associated with the diurnal cycle (not shown) are small almost everywhere so that the nighttime strengthening of the LLJ contributes strongly to the time-mean moisture transport only through its contribution to the time-mean flow pattern.

Profiles of the components of the time-mean horizontal (northward and eastward on sigma surfaces) flux vectors can be seen in Figs. 13c,d, which shows cross sections of the fluxes at 30°N together with contours of the mean meridional wind (in Fig. 13c only). It is evident that most of the moisture flux is confined to the lowest 100 mb or so of the atmosphere, including the strong low-level northward flux associated with the LLJ at 100°W and the strong southward flux on the West Coast associated with the northerly jet at about 120°W (shown in Fig. 13c) and the southeasterly transport by the transients other than the diurnal cycle between 100°W and 110°W (shown in Fig. 13d). The low-level southeasterly transport by the transients appears to be largely up the eastern slopes of the Rockies while the fluxes above that region tend to have a northerly component. There is little transport by the transients west of 110°W likely due in part to the relatively dry conditions over the high topography. The contribution from the diurnal cycle (not shown) is small everywhere.

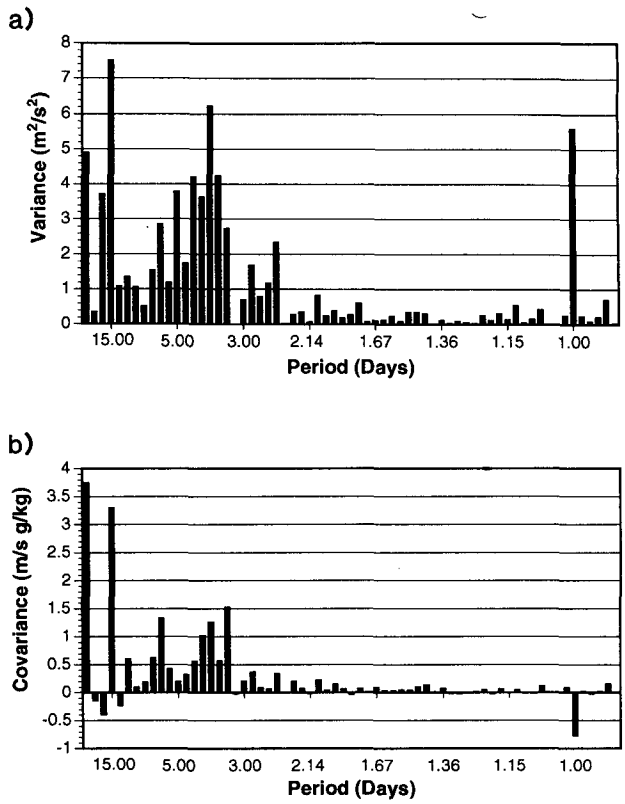

FIG. 14. The periodogram at 34°N, 100°W, σ = .97 (the second sigma level) of (a) the v wind (units are $m^2\ s^{-2}$) and (b) the northward moisture transport (units are $m\ s^{-1}\ g\ kg^{-1}$).

To look at the spectral signature of the transports in more detail, we focus on a point in the center of the LLJ at 34°N, 100°W, σ = .97. The variance spectrum for the v wind is shown in Fig. 14a. The strong diurnal signal is clearly evident. The magnitude of the diurnal component is similar to the individual contributions from the longer timescales. However, the total variance is dominated by synoptic and longer timescales. The variance spectrum for the specific humidity (not shown) is similar, but with a somewhat smaller contribution from the diurnal cycle relative to the low frequencies. The covariance spectrum for the northward moisture transport is shown in Fig. 14b. Surprisingly, the contribution from the diurnal component is southward; however, it is small compared to the northward transport by the synoptic and longer timescales.

These results suggest that the influence of the Great Plains LLJ on the time-mean moisture transport manifests itself in two ways. First, while the covariance of the diurnal components of the wind and moisture fluctuations does not contribute strongly to the total transport, the nighttime strengthening of the jet is very important to the total transport through its contribution to the time-mean flow pattern and, therefore, to its product with the time-mean moisture field. Thus, there

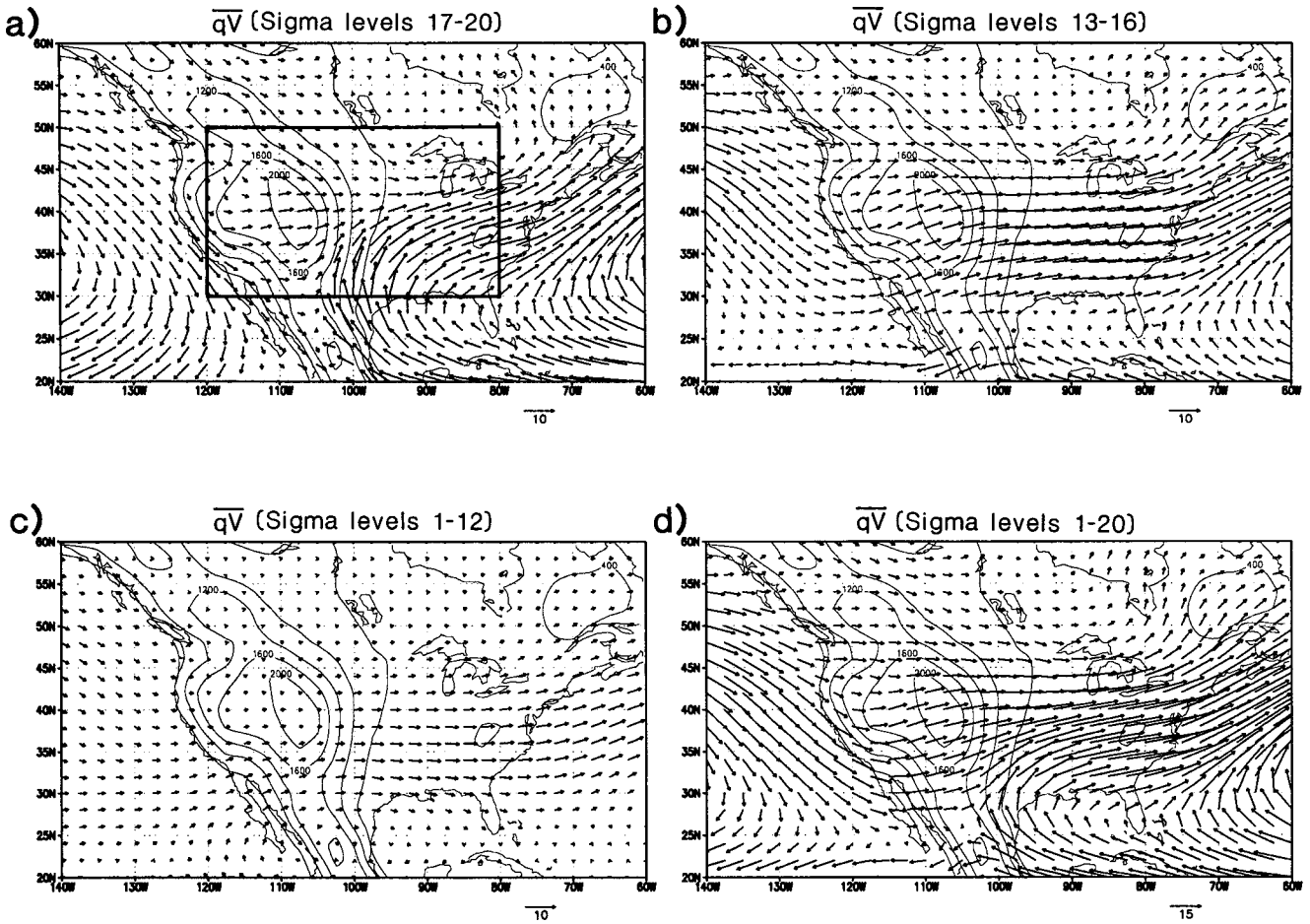

FIG. 15. Time-mean moisture flux for the two-month (May–June) model simulation for (a) the bottom 4 sigma levels (approximately 1000–850 mb), (b) the second 4 sigma levels (approximately 850–550 mb), (c) the top 12 sigma levels (approximately 550–10 mb), and (d) the vertical integral (sigma levels 1–20). Units are g kg^{-1} m s^{-1}. Note for comparison with Rasmusson (1968), the standard vector length in (d) is approximately 15×10^2 g cm^{-1} s^{-1}.

is a strong diurnal oscillation associated with the LLJ in the time series for total moisture transport as we shall see in the next section. Second, disruptions in the regular diurnal cycle of the jet, due to synoptic and longer timescale disturbances, which may enhance or reduce the strength of the jet, contribute strongly to the transient transport.

c. *Analysis of the moisture budget over the continental United States*

In this section we examine the simulated fluxes of moisture onto the continental United States at all atmospheric levels and compute the moisture budget for the region outlined in Fig. 15a, which corresponds approximately to the region studied by Rasmusson (1968). The fluxes are presented as vertical integrals over three different layers to highlight the differences of the transports in the low, middle, and upper levels of the atmosphere.

The four panels in Fig. 15 show the moisture fluxes vertically integrated over 1) the lowest 4 sigma layers (17–20, approximately from the surface to 850 mb), 2) the next 4 sigma layers (13–16, approximately from 850 to 550 mb), 3) the 12 uppermost sigma layers (1–12, approximately from 550 to 10 mb), and 4) the full vertical extent of the atmosphere. Figure 15a shows that the strongest flux onto the continent occurs at low levels over the south-central United States and northeastern Mexico. On the western boundary of the United States, the flow is primarily parallel to the continent with very little influx of moisture. Most of the flux onto the continent across the western boundary occurs between 850 and 550 mb. The east coast is characterized by a strong outflow in the lower and middle troposphere. These are generally consistent with the ob-

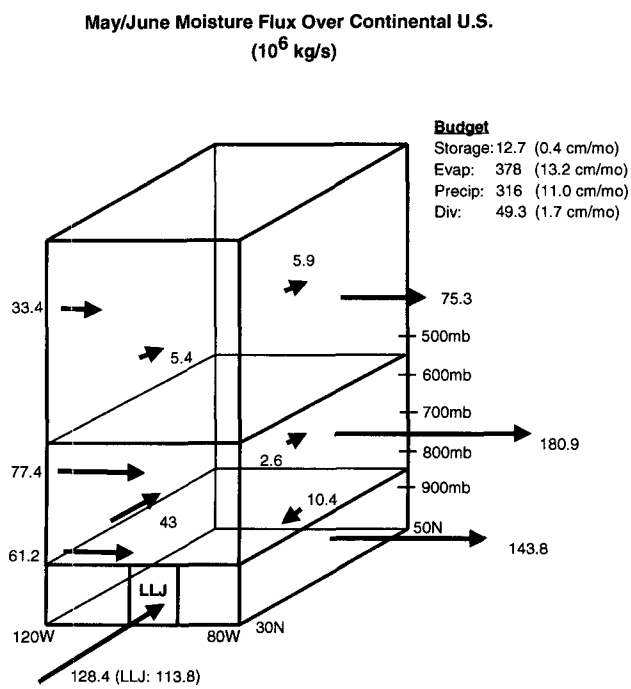

FIG. 16. Time-mean moisture flux and budget for the two-month (May–June) model simulation for the region outlined in Fig. 15a. Size of region is 7.54×10^6 km^2.

served vertically integrated moisture fluxes presented by Rasmusson (1967, see Figs. 5 and 6 in that study) that also show a strong northward flux onto the continent centered at about 27°N, 98°W and a strong outflow at the east coast. The maximum observed value of about 2400 g cm^{-1} s^{-1} for the vertically integrated moisture inflow occurs at 98°W, 27°N for July 1962 and is considerably larger than the largest simulated values of about 1000–1500 g cm^{-1} s^{-1} for May and June. The difference may be due in part to interannual variability; Benton and Estoque (1954), for example, show values in this region closer to 1000 g cm^{-1} s^{-1} for the summer of 1949, and Peixoto and Oort (1983) show long term averages (1963–73) of about 800 g cm^{-1} s^{-1} for June–August. Another source of the differences may be due to the differences in the vertical resolution of the datasets employed, which range from every 50 mb up to 250 mb for the Rasmusson (1967) study, to just four levels (surface, 850, 700, and 500 mb) for the Benton and Estoque (1954) study.

The overall moisture budget for the rectangular region approximately outlining the continental United States in Fig. 15a is shown in Fig. 16. The inflow from the southern boundary is dominated by that due to the mean low-level jet between about 102.5°W and 92.5°W. The other major source of moisture inflow is at the western boundary in the layer between 850 and 550 mb. The inflow associated with the LLJ accounts for one-third of the net moisture entering through the entire depth of the southern and western boundaries. Very little moisture enters or leaves through the northern boundary with most of the outflow occurring through the eastern boundary below 550 mb. There is a net divergence of moisture transport of 49.3×10^6 kg s^{-1} balanced by a net moisture source due to an excess of evaporation over precipitation of 62×10^6 kg s^{-1} minus a net moisture storage of 12.7×10^6 kg s^{-1}.

Though it is difficult to make an exact comparison, the values are similar to those found in the observations by Rasmusson (1967). The observed values show considerably less outflow from the east coast during May and June (400×10^6 kg s^{-1} simulated versus about 240×10^6 kg s^{-1} observed). However, there is a dramatic increase from 200×10^6 kg s^{-1} to more than 300×10^6 kg s^{-1} in the observations between May and July, which might suggest a considerable year-to-year variability in this quantity. The observations analyzed by Rasmusson (1967) also show significant outflow from the northern boundary, while the simulation shows a small inflow. The net divergence of 49.3×10^6 kg s^{-1} is somewhat large compared with Rasmusson (1967), which shows only a small divergence ($<20 \times 10^6$ kg s^{-1}) for the spring and summer months. This net divergence is composed of a net convergence of 56.2×10^6 kg s^{-1} in the lower layers, which is half the influx due to the LLJ by itself, and net divergences of 63.1×10^6 kg s^{-1} and 42.4×10^6 kg s^{-1} in the middle and upper layers, respectively. Both the evaporation and precipitation appear to be large compared with observations. [Rasmusson (1968), for example, gives May/June precipitation of 8.3 cm month^{-1} and evaporation of 7.16 cm month^{-1} (for the central plains and eastern United States).] Similar values are given in Benton and Estoque (1954) for North America, but in that study evaporation slightly exceeds precipitation.

Figure 17 is similar to Fig. 15 except that it shows the difference between nighttime and daytime fluxes of moisture, where the nighttime is defined as 1800 CST to 0600 CST and the daytime is defined as 0600 CST to 1800 CST. The night minus day signal is substantial at low levels (Fig. 17a) over much of the continent with the largest differences being those associated with the nocturnal inland flow of the Great Plains LLJ just east of the Rockies and extending from 20°N to about 35°N. There is also a significant diurnal oscillation in low-level fluxes over the midwestern and eastern U.S., particularly over the east coast where the nocturnal excess of westerly fluxes changes over to an excess of northwesterlies, and along the west coasts of the United States and Mexico. At intermediate (Fig. 17b) and upper levels (Fig. 17c), the major signal is centered at about 100°W and located roughly between 20° and 40°N with some additional signal over Baja California at middle levels and the midatlantic coast

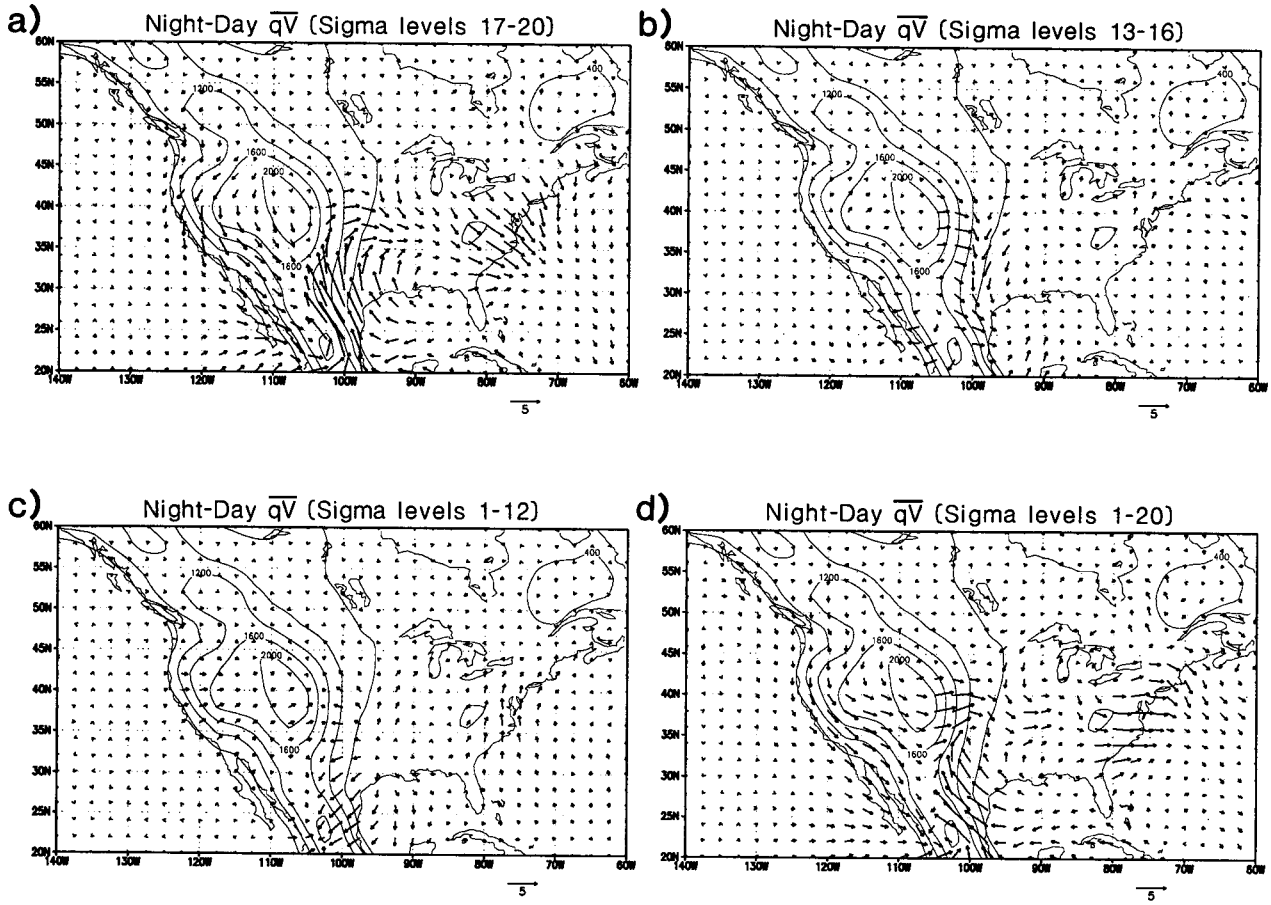

FIG. 17. Same as Fig. 15 except for night (1800–0600 CST) -day (0600–1800 CST).

of the United States at upper levels. The vertically integrated night–day moisture flux (Fig. 17d) reflects the low-level flow. The direction and magnitude of the night minus day flux east of the Rocky Mountains is similar to that found by Rasmusson (1967, see Fig. 31). In particular, that study also found a relative inflow during the night over the south-central United States and Mexico and outflow off the east coast. On the other hand, the coherent simulated northerly night minus day flux on the West Coast is not evident in the observations. Rasmusson (1967) also found that the night minus day fluxes in the middle troposphere tend to be out of phase with those at low levels over the south-central and southeastern United States, in concordance with the discussion of section 3d.

The primary signals in the night minus day differences for the overall moisture budget (Fig. 18) for the rectangular region representing the continental United States are a nocturnal excess of inflow across the southern boundary associated with the LLJ and a nocturnal excess of outflow through the eastern boundary, also in the lowest levels. The moisture inflow due to the LLJ is over 1.6 times as large during the night as during the day. Other significant flux differences are the northerly excess of nocturnal flux across the southern boundary in the middle and high layers, and a westerly excess of nocturnal flux across the western boundary at high levels. There is a large diurnal cycle in moisture storage for the rectangular region with an amplitude more than 13 times the size of the daily average storage. This diurnal cycle, which consists of a net moisture sink during the nighttime hours and a net source during the day, is driven by a huge diurnal cycle in evaporation, in which only about 8% of the daily total evaporation occurs during the nighttime hours. This is partially countered by a large diurnal cycle in precipitation in which only 28% of the total precipitation occurs at night so that there is a net nighttime deficit of evaporation minus precipitation of 115×10^6 kg s^{-1} and a net daytime excess of this difference of 239×10^6 kg s^{-1}. The vertical profile of the divergence does not change in sign from day to night, but the low-level convergence increases by 40% from its daytime value and the middle-level divergence increases by a little

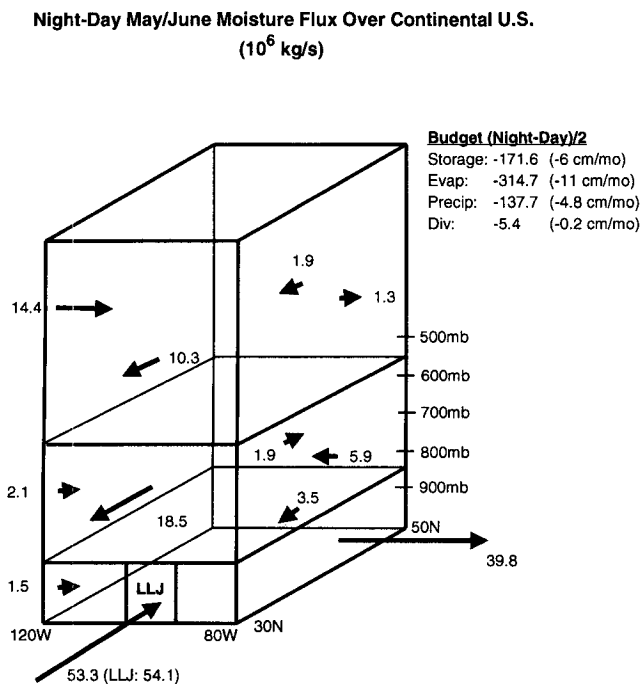

FIG. 18. Same as Fig. 16 except for night (1800–0600 CST) -day (0600–1800 CST).

over 20%, while the net column-integrated divergence decreases by 20% from its daytime value.

5. Summary and discussion

A two-month, springtime simulation with the 2° × 2.5°, 20-level GEOS-1 AGCM has produced a Great Plains low-level jet with a vertical and temporal structure, directionality, and climatological distribution that compare favorably with the limited observational basis that is available for this phenomenon. The simulated LLJ is evident in the time series of wind-speed profiles for individual grid points in the region as a low-level, quasi-regular, nocturnal peak in wind speed, generally located a few hundred meters above the ground.

The simulated LLJ and its diurnal cycle are part of a striking and coherent phenomenon on the subcontinental scale. This phenomenon involves the convergence of low-level easterlies over the Mexican Plateau each evening from the Gulf of Mexico and of low-level westerlies from Baja California and the Pacific Ocean. The easterlies turn anticyclonically toward the north to form the Great Plains low-level jet. This pattern can be interpreted as the nightly intrusion, as surface friction decreases, of the Atlantic anticyclonic, subtropical gyre (associated with the Bermuda high) onto the North American continent. It is a much more regular phenomenon, especially in subtropical regions such as the Gulf Coast of Mexico, than is apparent at individual extratropical locations such as Forth Worth, where there is considerable local variability on the synoptic timescale.

The model has also simulated a pair of northerly LLJ frequency maxima off the California coast and at the eastern extent of the east Pacific anticyclonic, subtropical gyre. These maxima seem to correspond to observations of a so-called "Baja Jet." This flow exhibits less of a diurnal variation than the Great Plains LLJ because it occurs for the most part over open ocean where diurnal variations in surface friction and heat flux are much less pronounced than over land. There is, however, a strong diurnal signal at the extreme eastern edge of the east Pacific gyre in the vicinity of Baja California due to the diurnal variations of fluxes over the land surface.

These diurnal cycles in the low-level flow give rise to a characteristic diurnal cycle in low-level divergence. The simultaneous acceleration of the low-level easterlies and southerlies of the Atlantic gyre and the low-level westerly acceleration over the western United States and the western parts of Mexico in the evening hours results in marked low-level convergence over the eastern slopes of the U.S. Rockies and over the Mexican High Plateau, with enhanced divergence in the Gulf of Mexico and off the Pacific coast of the United States and Mexico. Anticyclonic turning of wind direction during the night results in a phase shift of of the divergence pattern over central Mexico and a weakening of the convergence over the Great Plains. By noon, the low-level divergence pattern over land surfaces virtually disappears.

While the diurnal signal over the United States and northern Mexico is strongest at low levels, it also extends into the middle and even the upper troposphere in some regions, in agreement with the observational evidence of Borden and Hering (1962). The vertically alternating sign of the diurnal signal appears to represent a "thermal chimney" in which daytime heating and nighttime cooling over the high terrain is responsible for setting up a vertically and temporally varying pattern of anomalous inflow and outflow in that region.

The time-averaged climatological picture of the low-level flow is dominated over land by the nocturnal phase of the diurnal cycle, in which surface friction is minimal and wind speeds are strongest. The continental penetration by the Atlantic gyre clashes with the east Pacific gyre over the Mexican Plateau and with the westerlies in the lee of the U.S. Rockies, but less abruptly in the time mean than in the nocturnal phases. This pattern, with its zones of strong convergence, is characteristic of an unsteady, strongly forced flow. Over the open ocean, the mean low-level flow is more reminiscent of a smooth, climatological pattern.

Success in reproducing the essential properties of the Great Plains LLJ with the GEOS-1 AGCM will allow us to carry out experiments that can help establish

the basic cause or causes of the LLJ. The Great Plains LLJ seems to be a feature of a larger-scale phenomenon. Namely it is the southerly flowing branch of a low-level subtropical Atlantic gyre. The existence of this gyre and of the East Pacific gyre appears to be at least partially due to the interruption of the subtropical band of easterlies by the Mexican isthmus. This may be due to heating over Mexico, to the blocking effect of the mountains, or to both. We hope to help determine this by running a set of experiments in which we remove the heating, the mountains, or both. The diurnal cycle in low-level flow appears to be most strongly related to the diurnal cycle in surface friction rather than that of surface heating, since the phase of the flow seems to be consistent with that of friction. We plan to test this hypothesis by running experiments where the diurnal variations of friction alone or heating alone are suppressed. We also plan to investigate the importance of the diurnal cycle to the existence and structure of the LLJ by running an experiment in which we suppress the diurnal cycle to see if the low-level flow differs appreciably from the diurnally averaged flow shown in Fig. 12a.

Analysis of the moisture budget for the continental United States reveals the important role of the Great Plains low-level jet in transporting moisture from the Gulf of Mexico onto the continent. The lower atmosphere, below about 850 mb, is the dominant source of moisture influx over the continent with well over half of the total influx coming in at those levels. More than half of the influx at those levels, or nearly one-third of the influx at all levels, is attributable to the Great Plains LLJ. Nearly two-thirds of the flux due to the LLJ or one-fifth of the influx at all levels can be attributed to the nocturnal phase alone of the LLJ due to its dominance in the computation of the time-averaged low-level flow. Spectral decomposition in time of the moisture transport associated with the jet shows that it is the mean flow pattern and not covariances associated with the diurnal cycle that contribute most significantly to the total time-mean moisture transport. In fact, the covariances on the diurnal timescale are negative and negligible despite the strong diurnal signal in the wind. Covariances on the synoptic and longer timescales contribute about one-fifth of the total time-mean transport of moisture in the jet region.

Comparison between the present simulation and the Bonner climatology is very good despite the disparity in the averaging periods. LLJ frequency maxima are aligned along similar axes, and quantitatively, the peak frequencies are reasonably close to one another with the simulation giving higher values by about 10%. The Bonner climatology exhibits a double maximum of frequency, while the simulation exhibits a single elongated peak. These differences between the simulation and the observations might be resolved by extending the integration to include the more quiescent late fall, winter, and early spring periods. The higher jet frequencies of the simulation would surely become lower in this case, and individual frequency peaks from different periods of the annual cycle might appear simultaneously. Consequently, we plan to carry out a longer, multiyear integration with the GEOS-1 AGCM in the near future to assure our confidence in its ability to simulate the Great Plains LLJ in both the simulation mode and the assimilation mode, and to provide a more comprehensive dataset for the study of its properties and interpretation.

In addition to our studies on the mechanisms possibly responsible for the jet and our investigation with the multiyear integration discussed above, we will examine the simulation of low-level jets in other regions where they are known to occur with some regularity, such as to the east of the Andes Mountains, and we will analyze the variability of the LLJ and its interaction with the large-scale flow.

The current effort to produce a five-year assimilated dataset using the GEOS AGCM (Schubert et al. 1993) should allow a much improved description of the Great Plains LLJ, its role in the moisture budget of the United States, and how it interacts with the large-scale flow. Preliminary results from the assimilation for May and June of 1988 are encouraging.

Acknowledgments. We wish to acknowledge the key role of Andrea Molod in the development and implementation of the planetary boundary layer into the GEOS AGCM. Thanks also go to Chung-Yu Wu and David Case for their help in data processing, and Laura Rumburg for her help in drafting the figures. Richard Rood provided much valued encouragement, and helpful comments on an early version of the paper. This work was supported by NASA's Earth Observing Systems (EOS) projects on 4D Data Assimilation and Computing. David Case was supported under the EOS project on Global Hydrological Processes and Climate.

APPENDIX

The Surface Layer and the Turbulent Length Scale

The Monin–Obukov similarity functions that are used in conventional atmospheric models realistically represent the vertical structure of only the "surface layer" or "constant-flux layer," which extends a few tens of meters above the ground. The Monin–Obukov similarity functions for the GEOS model have been selected to realistically represent the vertical structure of an "extended surface layer" that can be as deep as 150 m. Under neutral conditions and over reasonably homogeneous terrain, according to Panofsky (1973), observed wind profiles between 30 and 150 m remain close to logarithmic because the nonlinear decrease of the mixing length above the surface layer compensates for the decrease of stress with height. When the surface

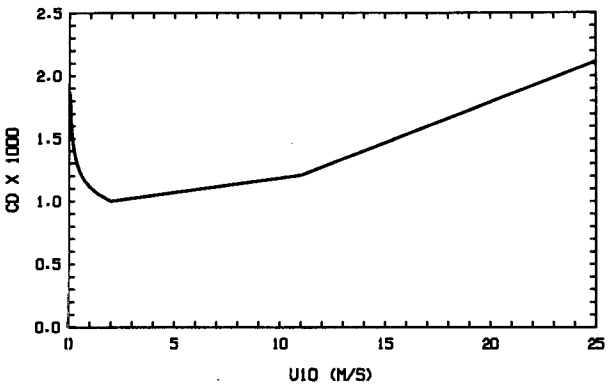

FIG. A.1. Roughness length z_0 over sea surfaces as a function of the surface-stress velocity u_*, shown as the relationship between the 10-m neutral drag coefficient (derived from z_0) and the 10-m wind (derived from u_* and z_0). The function is an interpolation between the 10-m drag coefficient and wind relation of Large and Pond (1981) for moderate to large wind speeds and the reciprocal z_0–u_* relationship of Kondo (1975) for weak wind speeds (or aerodynamically smooth surfaces).

layer is unstable, Panofsky (1973) claims that the KEYPS function

$$\phi_m^4 - 18\zeta\phi_m^3 = 1 \qquad \text{(A1)}$$

adequately represents the Monin-Obukov similarity structure for momentum up to 150 m.

This function and its generalization for scalar quantities

$$\phi_h^2 - 18\zeta\phi_h^3 = 1 \qquad \text{(A2)}$$

are used in the GEOS AGCM to interpolate between the near-surface behavior (small values of $-\zeta$) described by the functions of Businger et al. (1971) and the convective limit

$$\phi_{m,h} \rightarrow |\zeta|^{-1/3}, \qquad \text{(A3)}$$

far from the surface (large values of $-\zeta$) where unstable stratification dominates over shear. In this limit, the (virtual) potential temperature gradient depends only on (virtual) heat flux and not on stress. Another advantage of this choice of the similarity functions (A1) and (A2) is that in the limit of vanishing surface wind, their limiting behavior (A3) predicts nonvanishing surface heat and moisture fluxes. In this case, the coefficient C_H of heat exchange and the drag coefficient C_D are proportional to the 1/2 power of the negative of the bulk Richardson number Ri_b for the surface layer, and the surface (virtual) heat flux is proportional to the 3/2 power of the negative of the change of (virtual) potential temperature. In other words, the magnitude of the Brunt–Väisälä frequency times the depth of the surface layer replaces surface wind as the ventilation factor for surface exchanges.

The stability functions chosen for the stable surface layer are the ones suggested for scalar quantities by Clarke (1970) on the basis of his work with the Wangara dataset

$$\phi_h = \frac{1 + 5\zeta_1}{1 + 0.00794\zeta(1 + 5\zeta_1)},$$

$$\text{where} \quad \zeta_1 = \min(\zeta, 1), \qquad \text{(A4)}$$

and a slightly modified version for momentum

$$\phi_m = \frac{1 + 5\zeta_1}{1 + 0.00794\zeta_1(1 + 5\zeta_1)}. \qquad \text{(A5)}$$

Over land surfaces, the surface roughness is assumed to be a (time dependent) function of vegetation type as prescribed by the Simple Biosphere dataset of Sellers et al. (1986). Over sea surfaces, the roughness length is computed as a function of the surface-stress velocity u_*. The functional relationship between z_0 and u_* is an interpolation between the relation of Large and Pond (1981) for moderate to large wind speeds and the reciprocal relationship of Kondo (1975)

$$z_0 = \frac{c}{u_*} \qquad \text{(A6)}$$

for weak wind speeds (or aerodynamically smooth surfaces). The relationship is shown in Fig. A1 with the 10-m neutral drag coefficient (derived from z_0) as a function of the 10-m wind (derived from u_* and z_0). Both u_* and z_0 are calculated over sea surfaces in the GCM by the method of numerical iteration. Over ice, the roughness parameter is fixed at 0.1 mm.

The difference between roughness lengths for scalar exchange and for momentum exchange is expressed in the GEOS-1 AGCM via the definition of a viscous sublayer. Temperature and moisture exchange between the surface and the air immediately above it is accomplished by molecular viscosity, while the exchange of momentum is accomplished largely by the form drag of the roughness elements. The dimensionless change in any scalar quantity S over the depth of the essentially laminar region just above the earth's surface, where molecular viscosity is dominant and gradients of scalars are the largest, is formulated as

$$\frac{\Delta S}{S_*} = 0.55\left(\frac{u_* h_0}{\nu}\right)^{1/2}(\mathrm{Pr}^{2/3} - 0.2), \qquad \text{(A7)}$$

where h_0 is the roughness element size taken to be the smaller of 10 z_0 or 1 cm, ν is the molecular viscosity of air and Pr is the molecular Prandtl number for air. Equation (A7) is based on a relation given by Yaglom and Kader (1974). This quantity is added to the integral $\int \phi_h/kzdz$ in the determination of the flux-profile relationship for heat and moisture. The impact of the viscous sublayer parameterization on GEOS-1 GCM simulations will be discussed in a future paper.

The PBL consists of those model layers adjacent to the ground where TKE is significant with ℓ increasing with increasing depth of the PBL, but the turbulent length scale formulation also applies to elevated layers that are disjoint from the PBL, even when those layers are statically stable. The turbulent length scale ℓ at a height z above the ground is given by the formula of Blackadar,

$$\ell = \frac{kz\ell_0}{kz + \ell_0}, \tag{A8}$$

except that when z is contained within an unstable ($\mathrm{Ri} < \mathrm{Ri}_{cr}$) model layer, ℓ_0 is defined as the depth of the unstable atmospheric layer (consisting of one or more contingent model layers which are unstable), which contains that model layer. The upper and lower boundaries of that unstable atmospheric layer are determined by vertical interpolation of

$$S = \frac{g\dfrac{\partial\theta_v}{\partial z}}{\theta_{v0}} - \mathrm{Ri}\left|\frac{\partial U}{\partial z}\right|^2. \tag{A9}$$

For stable layers of the model ($\mathrm{Ri} \geqslant \mathrm{Ri}_{cr}$), ℓ_0 has been defined as

$$\ell_0 = q[(S + q^2/\ell_{00}^2 + 10^{-20})]^{-1/2}, \tag{A10}$$

where $\frac{1}{2}q^2$ is the turbulent kinetic energy within the model layer, and ℓ_{00} is the depth that would have been assigned to the unstable atmospheric layer containing the model layer if the model layer itself had been unstable. Note that $\ell_0 \approx \ell_{00}$ for a near-neutral layer ($S \approx 0$) and that $\ell_0 \approx q/N$, where N is the Brunt–Vaisala frequency for a very stable layer (S very large).

REFERENCES

Arakawa, A., and W. Schubert, 1974: Interaction of a cumulus ensemble with the large-scale environment. Part I. *J. Atmos. Sci.*, **31**, 674–701.

——, and M. J. Suarez, 1983: Vertical differencing of the primitive equations in sigma coordinates. *Mon. Wea. Rev.*, **111**, 34–45.

Astling, E. G., J. Paegle, E. Miller, and C. J. O'Brien, 1985: Boundary layer control of nocturnal convection associated with a synoptic scale system. *Mon. Wea. Rev.*, **113**, 540–552.

Benton, G. S., and M. A. Estoque, 1954: Water-vapor transfer over the North American continent. *J. Meteor.*, **11**, 462–477.

Blackadar, A. K., 1957: Boundary layer wind maxima and their significance for the growth of nocturnal inversions. *Bull. Amer. Meteor. Soc.*, **38**, 283–290.

Bleeker, W., and M. J. Andre, 1951: On the diurnal variations of precipitation, particularly over central U.S.A., and its relation to large-scale orographic circulation systems. *Quart. J. Roy. Meteor. Soc.*, **77**, 260–271.

Bonner, W. D., 1968: Climatology of the low level jet. *Mon. Wea. Rev.*, **96**, 833–850.

——, and J. Paegle, 1970: Diurnal variations in the boundary layer winds over the south-central United States in summer. *Mon. Wea. Rev.*, **98**, 735–744.

Burridge, D. M., and J. Haseler, 1977: A model for medium range weather forecasting–adiabatic formulation. Tech. Rep. No. 4, European Centre for Medium Range Weather Forecasts, Bracknell, Berkshire, United Kingdom, 46 pp.

Businger, J. A., J. C. Wyngaard, Y. Izumi, and E. F. Bradley, 1971: Flux profile relationships in the atmospheric surface layer. *J. Atmos. Sci.*, **28**, 181–189.

Chou, M. D., 1984: Broadband water vapor transmission functions for atmospheric IR flux computations. *J. Atmos. Sci.*, **41**, 1775–1778.

——, and L. Peng, 1983: A parameterization of the absorption in the 15 μm CO_2 spectral region with application to climate sensitivity studies. *J. Atmos. Sci.*, **40**, 2183–2192.

Clarke, R. H., 1970: Observational studies in the atmospheric boundary layer. *Quart. J. Roy. Meteor. Soc.*, **96**, 91–114.

Davies, R., 1982: Documentation of the solar radiation parameterization in the GLAS climate model. NASA Tech. Memo. 83961, 57 pp.

Fast, J. D., and M. D. McCorcle, 1990: A two-dimensional numerical sensitivity study of the Great Plains low-level jet. *Mon. Wea. Rev.*, **118**, 151–163.

Harshvardhan, R. Davies, D. A. Randall, and T. G. Corsetti, 1987: A fast radiation parameterization for atmospheric circulation models. *J. Geophys. Res.*, **92**, 1009–1016.

Helfand, H. M., 1985: A new scheme for the parameterization of the turbulent planetary boundary layer in the GLAS fourth order GCM. Preprints, *Seventh Conf. Numerical Weather Prediction*, Montreal, Quebec, Canada, Amer. Meteor. Soc., 348–354.

——, and J. C. Labraga, 1988: Design of a nonsingular level 2.5 second-order closure model for the prediction of atmospheric turbulence. *J. Atmos. Sci.*, **45**, 113–132.

Hering, W. S., and T. R. Borden, 1962: Diurnal variations in the summer wind field over the central United States. *J. Atmos. Sci.*, **19**, 81–86.

Hoecker, W. J., 1963: Three southerly low-level jet systems delineated by the Weather Bureau special pibal network of 1961. *Mon. Wea. Rev.*, **91**, 573–582.

——, 1965: Comparative physical behavior of southerly boundary layer jets. *Mon. Wea. Rev.*, **91**, 133–144.

Holton, J. R., 1967: The diurnal boundary layer wind oscillation above sloping terrain. *Tellus*, **19**, 199–205.

Izumi, Y., and M. L. Barad, 1963: Wind and temperature variations during development of a low-level jet. *J. Appl. Meteor.*, **2**, 668–673.

Joseph, J. H., W. J. Wiscombe, and J. E. Weinman, 1976: The delta-Eddington approximation for radiative flux transfer. *J. Atmos. Sci.*, **33**, 2452–2459.

King, M. D., and Harshvardhan, 1986: Comparitive accuracy of selected multiple scattering approximations. *J. Atmos. Sci.*, **43**, 784–801.

Kondo, J., 1975: Air–sea bulk transfer coefficients in diabatic conditions. *Bound.-Layer Meteor.*, **9**, 91–112.

Krishna, K., 1968: A numerical study of the diurnal variation of meteorological parameters in the planetary boundary layer. I. Diurnal variations of winds. *Mon. Wea. Rev.*, **96**, 269–276.

Lacis, A. A., and J. E. Hansen, 1974: A parameterization for the absorption of solar radiation in the earth's atmosphere. *J. Atmos. Sci.*, **31**, 118–133.

Large, W. G., and S. Pond, 1981: Open ocean momentum flux measurements in moderate to strong winds. *J. Phys. Oceanogr.*, **11**, 324–336.

McCorcle, M. D., 1988: Simulation of surface-moisture effects on the Great Plains low-level jet. *Mon. Wea. Rev.*, **116**, 1705–1720.

McNider, R. T., and R. A. Pielke, 1981: Diurnal boundary-layer development over sloping terrain. *J. Atmos. Sci.*, **38**, 2198–2212.

Means, L. L., 1952: On thunderstorm forecasting in the central United States. *Mon. Wea. Rev.*, **80**, 165–189.

——, 1954: A study of the mean southerly wind—Maximum in low levels associated with a period of summer precipitation in the Middle West. *Bull. Amer. Meteor. Soc.*, **35**, 166–170.

Moorthi, S., and M. J. Suarez, 1992: Relaxed Arakawa–Schubert: A parameterization of moist convection for general circulation models. *Mon. Wea. Rev.*, **120,** 978–1002.

Paegle, J., and D. W. McLawhorn, 1983: Numerical modeling of diurnal convergence oscillations above sloping terrain. *Mon. Wea. Rev.*, **111,** 67–85.

——, J. N. Paegle, M. McCorcle, and E. Miller, 1984: Diagnoses and numerical simulation of a low-level jet during ALPEX. *Beitr. Phys. Atmos.*, **57,** 419–430.

Panofsky, H. A., 1973: Tower micrometeorology. *Workshop on Micrometeorology,* D. A. Haugen, Ed., Amer. Meteor Soc., 151–176.

Peixoto, J. P., and A. H. Oort, 1983: The atmospheric branch of the hydrological cycle and climate. *Variations in the Global Water Budget.* A. Street-Perrott et al. Eds., D. Reidel, 5–65.

Pitchford, K. L., and J. London, 1962: The low-level jet as related to nocturnal thunderstorms over midwest United States. *J. Appl. Meteor.*, **1,** 43–47.

Rasmusson, E. M., 1967: Atmospheric water vapor transport and the water balance of North America: Part I. Characteristics of the water vapor flux field. *Mon. Wea. Rev.*, **95,** 403–426.

——, 1968: Atmospheric water vapor transport and the water balance of North America: II. Large-scale water balance investigations. *Mon. Wea. Rev.*, **96,** 720–734.

Rodgers, C. D., 1968: Some extensions and applications of the new random model for molecular band transmission. *Quart. J. Roy. Meteor. Soc.*, **94,** 99–102.

Rosenfield, J. E., M. R. Schoeberl, and M. A. Geller, 1987: A computation of the stratospheric diabatic circulation using an accurate radiative transfer model. *J. Atmos. Sci.*, **44,** 859–876.

Sadourney, R., 1975: The dynamics of finite difference models of the shallow water equations. *J. Atmos. Sci.*, **32,** 680–689.

Schemm, J.-K., S. Schubert, J. Terry, S. Bloom, and Y. Sud, 1992: Estimates of monthly mean soil moisture for 1979–89. NASA Tech. Memo. 104571.

Schubert, S., J. Pfaendtner, and R. Rood, 1993: An assimilated dataset for earth science applications. *Bull. Amer. Meteor. Soc.*, **74,** 2331–2342.

Sellers, P. J., Y. Mintz, Y. C. Sud, and A. Dalcher, 1986: A simple biosphere Model (SiB) for use within general circulation models. *J. Atmos. Sci.*, **43,** 505–553.

Suarez, M. J., and L. Takacs, 1993: Documentation of the ARIES/GOES Dynamical Core Version 2. [Source and documentation available from M. Suarez, NASA/GSFC, Code 913, Greenbelt, MD 20771 (suarez@maxs.gsfc.nasa.gov).]

Sud, Y., and A. Molod, 1988: The roles of dry convection, cloud-radiation feedback processes and the influence of recent improvements in the parameterization of convection in the GLA GCM. *Mon. Wea. Rev.*, **116,** 2366–2387.

U.S. Navy 1956: *Marine Climatic Atlas of the World.* Vol. II. *North Pacific Ocean.* Direction of the Chief of Naval Operations, NAVER 50-1C-529.

Wallace, J. M., 1975: Diurnal variations in precipitation and thunderstorm frequency over the conterminous United States. *Mon. Wea. Rev.*, **103,** 406–419.

Wexler, H., 1961: A boundary layer interpretation of the low-level jet. *Tellus,* **13,** 368–378.

Yaglom, A. M., and B. A. Kader, 1974: Heat and mass transfer between a rough wall and turbulent fluid flow at high Reynolds and Peclet numbers. *J. Fluid. Mech.*, **62,** 601–623.

Yamada, T., 1977: A numerical experiment on pollutant dispersion in a horizontally-homogeneous atmospheric boundary layer. *Atmos. Environ.*, **13,** 1015–1024.